Review

A Review of Aggregation-Based Colorimetric and SERS Sensing of Metal Ions Utilizing AuAg Nanoparticles

Shu Wang , Lin Yin * , Yanlong Meng , Han Gao , Yuhan Fu , Jihui Hu , Chunlian Zhan *

Posted Date: 19 January 2026

doi: 10.20944/preprints202601.1310.v1

Keywords: Au/Ag nanoparticles; surface-enhanced Raman scattering (SERS); colorimetric sensing; metal ions; aggregation; localized surface plasmon resonance (LSPR)

 doi:10.20944/preprints202601.1310.v1

Review

A Review of Aggregation-Based Colorimetric and SERS Sensing of Metal Ions Utilizing Au/Ag Nanoparticles

Shu Wang, Lin Yin *, Yanlong Meng, Han Gao, Yuhan Fu, Jihui Hu and Chunlian Zhan *

China Jiliang University, Hangzhou 310018, China

* Correspondence: 22A0405204@cjlu.edu.cn (L.Y.); 20a0405185@cjlu.edu.cn (C.Z.)

Abstract

The accurate monitoring and dynamic analysis of metal ions are of considerable practical significance in environmental toxicology and life sciences. Colorimetric analysis and surface-enhanced Raman scattering (SERS) sensing technologies, utilizing the aggregation effect of gold and silver nanoparticles (Au/Ag NPs), have emerged as prominent methods for rapid metal ion detection, serving as effective complements to conventional bulky instrumental analysis techniques. This is propelled by their distinctive localized surface plasmon resonance (LSPR) response and electromagnetic field enhancement mechanisms. This article evaluates contemporary optical sensing methodologies utilizing aggregation effects and their advancements in the detection of diverse metal ions. It comprehensively outlines methodological advancements from nanomaterial fabrication to signal transduction, encompassing approaches such as biomass-mediated green synthesis and functionalization, targeted surface ligand engineering, digital readout systems utilizing intelligent algorithms, and multimodal synergistic sensing. Recent studies demonstrate that these techniques have attained trace-level identification of target ions regarding analytical efficacy, with detection limits generally conforming to or beyond applicable environmental and health safety regulations. Moreover, pertinent research has enhanced detection linear ranges, anti-interference properties, and adaptability for point-of-care testing (POCT), validating the usefulness and developmental prospects of this technology for analysis in complicated matrices.

Keywords: Au/Ag nanoparticles; surface-enhanced Raman scattering (SERS); colorimetric sensing; metal ions; aggregation; localized surface plasmon resonance (LSPR)

1. Introduction

Metal ions are omnipresent in the environment, prevalent in natural water bodies, soil matrices, and biological fluids. The real-time monitoring and accurate analysis of their concentrations are crucial for preserving global ecological balance, ensuring food safety, and enabling early clinical diagnosis [1]. In environmental toxicology, many heavy metal pollutants, including chromium (Cr^{3+}, Cr^{6+}), mercury (Hg^{2+}), and lead (Pb^{2+}), exhibit significant environmental persistence and bioaccumulation potential. Even at trace concentrations, these pollutants can bioaccumulate within the food chain, resulting in irreparable harm to the central nervous system and other essential organs [2,3]. In contrast, transition metal ions, such as copper (Cu^{2+}) and iron (Fe^{2+}, Fe^{3+}), are crucial for vital biological functions; nonetheless, deviations from normal physiological concentrations—either deficiency or excess—can lead to oxidative stress or cytotoxicity through the Fenton reaction. This imbalance is significantly associated with neurodegenerative disorders, such as Parkinson's disease [4,5]. Moreover, the ecological behavior and biological consequences of alkali metals (e.g., Na^{+}) related to osmotic control [6], potentially hazardous aluminum ions (Al^{3+}) [7], and emerging rare earth elements [8] necessitate thorough examination.

 doi:10.20944/preprints202601.1310.v1

Traditionally, extensive instrumental analysis methods—such as inductively coupled plasma mass spectrometry (ICP-MS) [9,10], inductively coupled plasma optical emission spectrometry (ICP-OES) [11], and atomic absorption spectroscopy (AAS)—have been considered the "gold standard" for the quantitative assessment of metal ions [12]. These techniques are distinguished by their exceptionally low detection limits, extensive linear ranges, and superior reproducibility. Nonetheless, their extensive applicability is significantly restricted by intrinsic limits, such as costly instrumentation, substantial size, elevated operational and maintenance expenses, and stringent sample pretreatment prerequisites (e.g., acid digestion). These limitations substantially impede their implementation for real-time monitoring in resource-constrained areas or during abrupt environmental pollution incidents. To overcome the limitations of conventional techniques, researchers have increasingly focused on creating more efficient and expedited detection methods. As a result, other innovative methodologies have arisen, including electrochemical analysis [13][14], fluorescent probe technology [15][16], surface-enhanced Raman scattering (SERS) [17], and colorimetric analysis [18]. These methods maintain excellent detection sensitivity while markedly decreasing reliance on extensive equipment, thereby offering viable options for the swift on-site detection of metal ions.

Colorimetric analysis and SERS sensing, which leverage the localized surface plasmon resonance (LSPR) characteristics of noble metal nanomaterials (e.g., Au, Ag), have attracted significant research interest due to their exceptional optical response capabilities. The core premise of colorimetric sensing entails converting the interaction between metal ions and nanoprobes into observable spectrum shifts or discernible color alterations. Contemporary construction methodologies involve morphology etching, dissolution, or amalgamation through the redox characteristics of target ions [19–21]; the generation of precipitates via specific recognition adsorption or in situ reactions between probe molecules and ions [22,23]; and ion-induced nanoparticle aggregation. Aggregation-based colorimetric detection is a crucial method for facilitating swift ion analysis. This technique utilizes metal ions to diminish inter-particle distances, hence inducing strong dipole-dipole interactions and plasmonic coupling phenomena. The physical coupling results in a notable red-shift and broadening of the LSPR absorption band, which is macroscopically observed as a change in solution color, thus offering dual modalities for instrumental spectral analysis and on-site visual detection of metal ions [24,25].

While colorimetry delivers accessible optical feedback, SERS technology with analogous nanostructured substrates adds an additional detection dimension for enhanced fingerprint identification and quantitative analysis of trace analytes in complicated matrices. Due to the limited Raman scattering cross-sections of most metal ions, SERS detection often depends on indirect sensing frameworks. Recent studies have established several sophisticated mechanisms, including signal amplification techniques leveraging aptamer-regulated nanozyme catalytic activity [26], recognition approaches employing generic ligands to interact with multiple metal ions for distinct spectral fingerprints [27,28], ratiometric sensing reliant on conformational switches of DNA nanostructures [29], and "signal-off" mechanisms predicated on competitive ligand desorption [30,31]. In addition to these ways, metal ion-induced controlled aggregation functions as an efficient building method. This method adjusts the density of electromagnetic "hotspots" by modifying the aggregation state of nanoparticles, thus controlling the enhancement factor (EF) to create "signal-on" or "signal-off" sensors. The sub-nanometer gaps created by dense packing in aggregates can produce an exponentially increasing local electromagnetic field, greatly enhancing the signal of Raman reporter molecules situated at the hotspots; in contrast, the disruption of these aggregated structures results in the loss of hotspots and signal attenuation. This exact manipulation of the "aggregation–hotspot–signal intensity" cascade process by physical coupling offers a high signal-to-noise ratio detection platform for trace metal ion analysis [32].

 doi:10.20944/preprints202601.1310.v1

2. Fundamentals of Aggregation-Based Detection

The identification of metal ions through Au/Ag nanoparticle aggregation involves four specific stages: nanomaterial synthesis, ion-interface interaction, optical signal transmission, and data processing. Gold or silver nanoparticles (Au/Ag NPs) with defined morphologies and consistent dimensions are often generated as substrates using chemical reduction or seed-mediated growth techniques [33–35]. The introduction of target metal ions induces specific physicochemical interactions with the surface ligands or electric double layers of the nanoparticles, disrupting the metastable equilibrium of the colloidal system and prompting the transition of particles from a dispersed to an aggregated state. This aggregation tendency significantly modifies the LSPR properties of the system. This is observed macroscopically as a shift and broadening of the absorption spectra, representing the colorimetric response [18,36]. At the microscopic level, the decrease in inter-particle distance promotes the creation of "hotspots" characterized by elevated electromagnetic field density within the interstices, leading to a significant amplification of SERS signals [32,37]. These optical responses are finally recorded by spectrum equipment or portable devices for the qualitative identification and quantitative study of target ions [38].

The mechanisms by which metal ions induce nanoparticle aggregation primarily encompass three categories of physicochemical processes. The primary factor is the reduction of electrostatic repulsion and the compression of the electric double layer. The introduction of exogenous metal ions elevates the ionic strength of the solution, compressing the electric double layer on the particle surface and screening surface charges, which facilitates van der Waals attraction to prevail and induce aggregation [39–41]. The second mechanism is coordination bridging-induced assembly. Metal ions serve as coordination centers by binding to functional ligands comprising sulfur, nitrogen, or oxygen modified on the particle surface, thereby creating a permanent bridging network that facilitates the proximity of particles [42,43]. The third mechanism is instability driven by oxidative etching. This technique utilizes the elevated redox potential of particular metal ions to facilitate the oxidation and partial dissolution of the nanoparticle surface or the degradation of stabilizing ligands. The etching impact undermines the integrity of the surface protective layer and diminishes surface potential, thereby compromising colloidal stability and inducing irreversible aggregation [44–46].

Recent methodological advancements in colorimetric detection span seven principal dimensions. Green synthesis strategies utilizing biomass employ natural plant extracts or biomass derivatives to act as reducing agents, stabilizers, and recognition ligands, thereby streamlining the synthesis process and incorporating inherent anti-interference properties. Ligand engineering encompasses not just individual ligands but also the design of synthetic small molecules, the use of biological macromolecules like DNA or enzymes, and the creation of dual-ligand synergistic systems to facilitate the exact capture and interfacial manipulation of specific ions. Special Response Mechanisms overcome the constraints of conventional electrostatically generated aggregation by employing several methods, such as metal ion-mediated lattice doping, oxidative etching, anti-aggregation kinetic regulation, and ligand-metal charge transfer (LMCT). Physical Assistance and Post-Treatment methods incorporate microwave or laser liquid ablation during the synthesis phase to improve reaction speeds and surface cleanliness, while employing pH-selective precipitation in the post-treatment phase to enhance colloidal purity. Smart Readout and Algorithmic Enhancement integrate smartphone photography technology with machine learning algorithms, including Random Forest and Support Vector Machines (SVM), to facilitate digital calibration and accurate quantification of signals in intricate lighting conditions. Solid-Phase Support and Phase Transition tackle the difficulties of storing and transporting liquid-phase colloids by implementing hydrogel three-dimensional networks or paper-based microfluidic chips, hence broadening the application contexts for Point-of-Care Testing (POCT). Multimodal sensing develops dual-mode sensing systems that utilize light/light (e.g., fluorescence-colorimetric) or light/electric mechanisms, while also incorporating catalytic degradation functions to achieve interactive signal verification and the integration of "diagnosis and therapy."

 doi:10.20944/preprints202601.1310.v1

The methodological approach for SERS detection encompass six key factors. Molecular Probe Engineering creates "beacons" by incorporating dyes or functional molecules with elevated Raman scattering cross-sections, formulating bifunctional molecular approaches that merge chelation with luminescence, alongside multi-component synergistic modification strategies to tackle the challenge of metal ions devoid of intrinsic Raman signals. Plasmonic nanohybrid design meticulously organizes the spatial distribution and stability of electromagnetic hotspots at the nanoscale by the fabrication of Au@Ag core-shell structures, core-satellite assemblies, or magnetic composites. Special Response Mechanisms employ dynamic chemical processes—such as metal ion-catalyzed Fenton-like reactions, DNAzyme cleavage, oxidative etching, or spintronic effects—to regulate the "signal-on" and "signal-off" phases of spectrum signals. Moreover, SERS research predominantly employs Green synthesis strategies and Multimodal sensing techniques akin to those utilized in colorimetry, utilizing biomass substrates or supplementary signals to improve detection effectiveness. Chemometrics-Assisted Analysis focuses on high-dimensional spectral data by employing genetic algorithms (GA) or partial least squares (PLS) to create predictive models, thereby addressing issues associated with non-linear signal responses during aggregation and interference from intricate matrix backgrounds.Figure 1 delineates a roadmap of recent achievements, summarizing the principal methodologies mentioned, and displaying the workflow from nanomaterial fabrication and mechanism manipulation to intelligent analytical readouts.

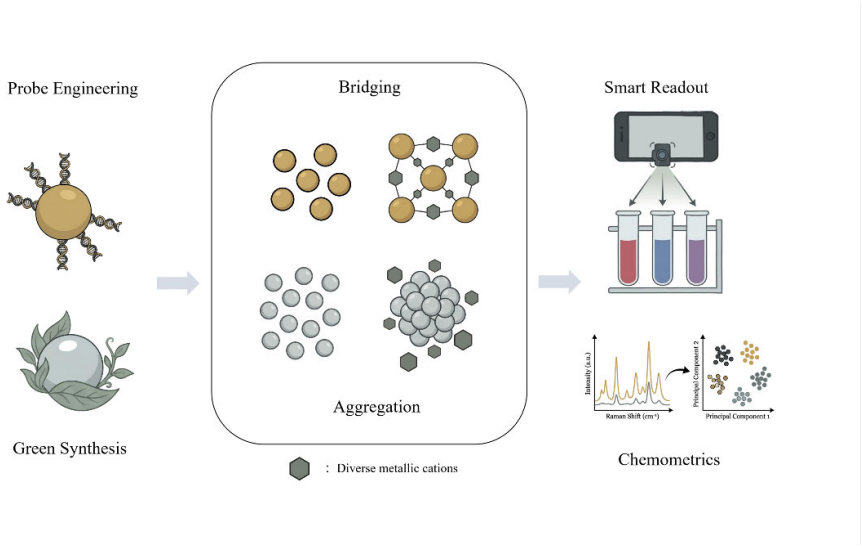

Figure 1. Schematic depiction of aggregation-based colorimetric and SERS sensing techniques for metal ions.

The varied advancements in synthesis methodologies, interfacial chemistry, and signal transduction processes mentioned above are primarily intended to exceed current detection limitations and improve the practicality and reliability of analytical procedures. The examined study exhibits excellent selectivity, accuracy, and reliability; nonetheless, they vary in the specific performance criteria prioritized for practical applications. This review utilizes unique tags to annotate pertinent material, so elucidating the distinct qualities of each contribution. In the realm of metal ion detection, "Ultrasensitive" refers to research that presents the lowest limit of detection (LOD), signifying a comparative benefit in trace analysis; "Wide linear range" implies studies that attain the most extensive linear response range among analogous assays. Concerning functional attributes, "Sensitive & Portable" denotes research that adeptly reconciles high sensitivity with on-site portability; "Self-calibrated" refers to systems equipped with signal self-calibration capabilities, effectively reducing environmental background interference to guarantee high reliability. Moreover, "High-stable" refers to research in which probes have been empirically validated to demonstrate considerable long-term storage stability.

 doi:10.20944/preprints202601.1310.v1

3. Colorimetric Sensors

3.1. Heavy Metal Ions

This section addresses the colorimetric detection of heavy metal elements, specifically chromium (Cr), mercury (Hg), and lead (Pb). The choice of surface-functionalization ligands is a crucial factor influencing the selectivity and sensitivity of AuNP-based colorimetric probes. Zhang et al. [47] extensively evaluated the efficacy of several surface ligands in their response to Cr^{3+}. The researchers developed a colorimetric probe utilizing 4-mercaptobenzoic acid (4-MBA) functionalized AuNPs and conducted a comparison with a 4-nitrothiophenol (4-NTP) device. Spectral analysis demonstrated that 4-MBA-modified AuNPs had the most pronounced absorbance variation and best sensitivity (Figure 2a). The detection method is attributed to ion-templated chelation, in which Cr^{3+} serves as a coordination center that precisely binds to the carboxyl groups on the AuNP surface. TEM imaging clearly demonstrated a transition of the nanoparticles from a monodispersed state to discrete aggregates upon the introduction of ions (Figure 2b), leading to a color change in the solution from wine-red to purple or blue. As the concentration of Cr^{3+} increased, the LSPR absorption band exhibited a consistent red-shift (Figure 2c). The absorbance ratio ($A_{635\ nm}/A_{520\ nm}$) exhibited a strong linear correlation in the range of 20–25 μM (Figure 2d), with a LOD of 5 μM.

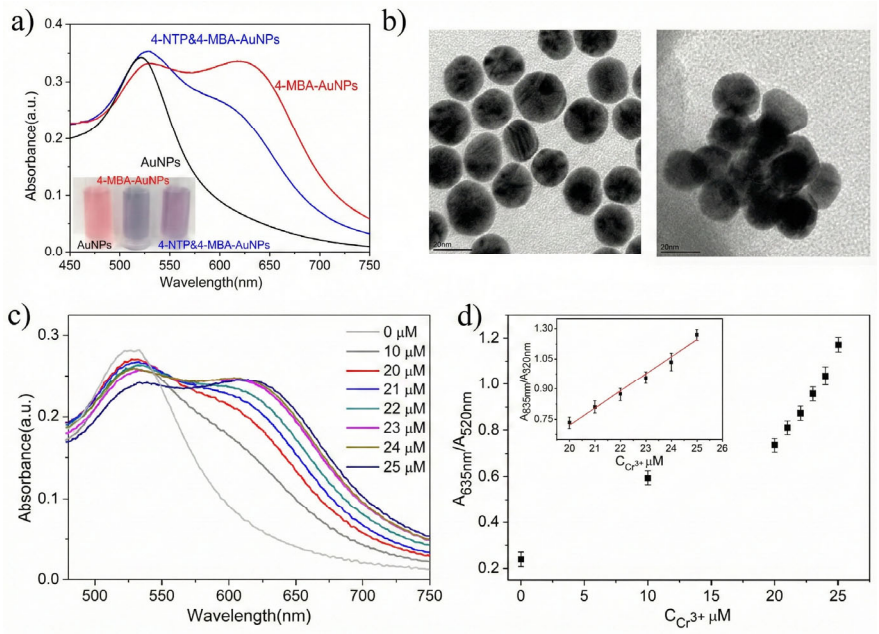

Figure 2. Evaluation and characterisation of the 4-MBA-AuNPs probe for the detection of Cr^{3+} [47].

The use of natural biomass for nanomaterial production offers a cost-effective method for detection. Memon et al. [48] utilized Ziziphus mauritiana leaf (ZmL) extract, abundant in carbonyl groups, as a reducing and capping agent to synthesize ZmL-AuNPs. The presence of Cr^{3+} dramatically enhanced the average size of the ZmL-AuNPs from 8 nm to 25 nm. This biosynthesized sensor attained a remarkably low limit of detection of 0.48 nM, with a linear range of 16–283 nM, and exhibited exceptional stability in complicated aqueous samples.

To address the performance constraints of individual nanomaterials, techniques using hybrid materials and multifunctional ligands have been developed. Shellaiah and Sun [49] ingeniously developed a hybrid probe that integrates cystamine-functionalized nanodiamonds (NDC) with AuNPs (NDC-AuNPs). This study utilized the extensive specific surface area and superior biocompatibility of NDCs as a carrier, facilitating aggregation through the coordination of surface amino/thiol groups with Cr^{3+}. This approach attained a sub-nanomolar limit of detection (0.236 nM)

 doi:10.20944/preprints202601.1310.v1

and a linear range of 10–400 nM, demonstrating commendable cyclic reversibility post-EDTA treatment.

Gunupuru and Paul [50] utilized amino-substituted 2-amino-5-mercapto-1,3,4-thiadiazole (AMT) to alter AuNPs, thereby creating a dual-functional colorimetric sensing platform. This method initially tethered AMT to the surface of gold nanoparticles by thiol groups, as depicted in Figure 3. In the presence of target ions, Cr^{3+} and Pb^{2+} interacted with surface amino groups, resulting in significant nanoparticle aggregation. This led to a redshift of the LSPR band and a color change from wine-red to blue. The approach attained limits of detection of 1.0 μM for Cr^{3+} and 0.4 μM for Pb^{2+} in the aqueous phase. Zhang et al. [51] developed a multifunctional platform utilizing ammonium thioglycolate (ATG) functionalized AuNPs. By employing various active sites (carboxyl groups and fluorine atoms) on the ATG surface, they accomplished the concurrent screening of moxifloxacin, ciprofloxacin, and Cr^{3+}. This platform displayed a limit of detection of 57.1 nM for Cr^{3+} with a linear response range of 0–5.0 μM, illustrating the adaptability of functionalized probes in the assessment of multi-component contaminants.

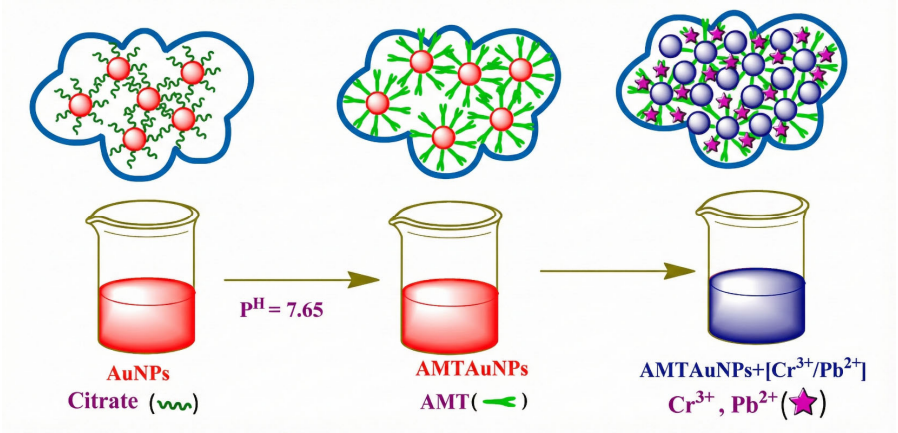

Figure 3. Schematic representation of the synthesis of AMT-functionalized AuNPs and the colorimetric detection technique for Cr^{3+} and Pb^{2+} [50].

To overcome the constraints of single-signal detection, Shi et al. [52] devised a dual-mode fluorescence/colorimetric sensing system utilizing carbon dots (CDs) and GSH-Au nanoparticles. The inner filter effect (IFE) facilitated Cr^{3+}-induced aggregation, producing a colorimetric signal while concurrently restoring the fluorescence of the CDs in a "turn-on" mode. At pH 5.4, the limits of detection for the fluorescence and colorimetric modalities were 0.31 μM and 0.30 μM, respectively, with linear ranges of 0.5–70 μM and 2–50 μM. This dual-mode cross-verification approach markedly improved data reliability in intricate matrices.

Algorithms embedded onto smartphones have become essential for swift on-site detection. Rajamanikandan et al. [53] created a portable platform integrated with smartphone RGB analysis. This platform utilized the significant reduction in surface potential (from -33.12 mV to -5.10 mV) resulting from the coordination of Cr^{3+} with MMT ligands to mitigate electrostatic repulsion—attaining an LOD of 12.4 nM (spectrophotometric LOD 6.93 nM, linear range 40–128 nM)—while also incorporating catalytic degradation capabilities, thereby preliminarily actualizing the concept of "theranostics" (diagnosis and therapy). To enhance integration and automation, Moradifar et al. [54] developed a microfluidic colorimetric chip utilizing polymethyl methacrylate (PMMA). The researchers methodically enhanced flow rate and pH parameters through a central composite design (CCD) model, addressing the problem of inconsistent mixing in conventional liquid-phase detection and minimizing reagent usage. The platform demonstrated a favorable linear response within the range of 1.00–35.00 μM, with a limit of detection of 0.33 μM, thereby affirming the practical utility of microfluidic technology for high-throughput on-site screening.

 doi:10.20944/preprints202601.1310.v1

Hexavalent chromium (Cr^{6+}) is a primary focus in water monitoring because of its significant carcinogenic properties and environmental durability. Sharma et al. [55] employed a microwave-assisted technique to swiftly synthesize chlorophyll-coated silver nanoparticles (Chl-AgNPs) in 10 seconds. This study utilized natural chlorophyll as a reducing and capping agent, leveraging its rich surface functional groups (such as methyl and carboxyl groups) as capture sites for Cr^{6+} to produce alterations in interparticle distance and aggregation. This was spectroscopically indicated by a red shift of the 410 nm characteristic peak and the appearance of a new peak at 357 nm. The sensor demonstrated excellent linearity throughout the 2–100 μM range (LOD 0.62 μM), and the distinct red color development effectively mitigated interference from As^{5+}. Skiba et al. [56] investigated the gas-liquid interfacial plasma discharge technique as an additional physical auxiliary strategy, successfully facilitating the one-pot fast synthesis of PVP-stabilized gold nanoparticles. This approach, leveraging the abundant active species and electron transfer produced during the plasma process, achieved synthesis within minutes without conventional reducing agents, guaranteeing exceptional surface purity of the nanoparticles. The study indicated a significant reliance of detection performance on pH: in acidic environments, Cr^{6+} predominantly exists as $HCrO_4^-$, resulting in strong electrostatic attraction to the protonated PVP surface and causing substantial aggregation; in contrast, under alkaline conditions, the electrostatic repulsion from the CrO_4^{2-} form impedes the signal. The revised mechanism enabled the sensor to provide a superior linear response within the range of 0.1–3.0 μM, with a limit of detection of 0.072 μM.

Muthwa et al. [57] adeptly integrated experimental characterisation with molecular dynamics (MD) simulations to elucidate ligand-ion interactions in a 1,5-diphenylcarbazide (DPC) functionalized gold nanoparticle system. The radial distribution function (RDF) study in the molecular dynamics simulation verified a significant attraction between Cr^{6+} and the nitrogen atoms in DPC, with a contact distance of around 3 Å. This interaction was markedly more potent than the binding force between DPC and the Au surface, resulting in ligand detachment from the nanoparticle surface. The AuNPs, shedding their protective coating, swiftly experienced uncontrolled aggregation, resulting in a color change of the solution from wine-red to blue. The LSPR peak exhibited a red shift from 520 nm and a reduction in intensity, while a new peak emerged at 670 nm. This approach attained a low limit of detection of 0.3 μM and incorporated smartphone-based CIE Lab* color space analysis, including hue angle and chroma. This method, in contrast to conventional absorbance techniques, yielded more comprehensive fingerprint data, hence enhancing theoretical insights into ligand-mediated aggregation behavior.

The elevated redox potential of Cr^{6+} can be further utilized to improve visual resolution. Karn-orachai et al. [58] conducted a comprehensive evaluation of the impact of various combinations of capping agents on probe performance (Figure 4). The comparative results indicated that only the bimetallic sol system, which combines Na-AuNPs and cit-AgNPs (Figure 4d), could facilitate a synergistic "oxidative etching-aggregation" mechanism. The potent Cr^{6+} initially oxidatively etched the AgNPs and AuNPs, resulting in the release of metal ions that caused significant aggregation and redeposition of the residual particles. This intricate chemical-physical process imparted the sensor with a spectrum of vivid color transitions—progressing from orange to deep reddish-purple, then to deep bluish-purple, and finally to gray as concentration escalated—significantly improving the resolution of unaided semi-quantitative analysis. The approach attained a LOD of roughly 0.44 μM (22.9 ppb) with a linear range of 0.05–50 ppm, showcasing distinct benefits in anti-interference efficacy and visual clarity.

 doi:10.20944/preprints202601.1310.v1

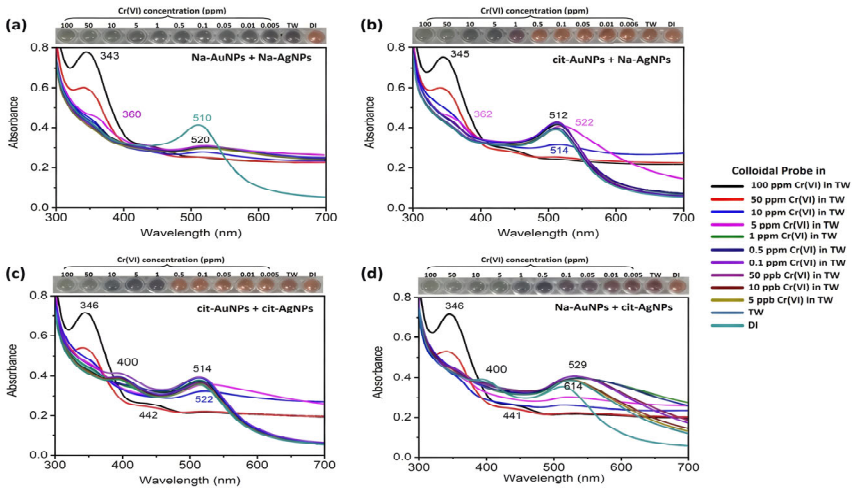

Figure 4. Comparative analysis of extinction spectra and perceptual color alterations in AuNP/AgNP mixes with varying capping agents following the addition of Cr^{6+} [58].

Table 1. Analytical efficacy of colorimetric tests for the identification of chromium ions (Cr^{3+} and Cr^{6+}).

Nanostructure	Ligand	Linear Range	LOD	Method	Evaluation	Ion	Ref.
AuNPs	4-MBA	20–25 μM	5 μM	Ligand Engineering	—	Cr^{3+}	[47]
ZmL-AuNPs	*Ziziphus mauritiana* extract	16–283 nM	0.48 nM	Green synthesis strategies	High-stable	Cr^{3+}	[48]
NDC-AuNPs	Cystamine-functionalized NDC	10–400 nM	0.236 nM	Ligand Engineering	Ultrasensitive	Cr^{3+}	[49]
AuNPs	AMT	—	1.0 μM	Ligand Engineering	—	Cr^{3+}	[50]
AuNPs	ATG	0–5.0 μM	57.1 nM	Ligand Engineering	—	Cr^{3+}	[51]
AuNPs & CDs	GSH	2–50 μM	0.30 μM	Multimodal sensing	Self-calibrated	Cr^{3+}	[52]
Metal NPs	MMT ligands	40–128 nM	12.4 nM	Smart Readout & Algorithmic Enhancement	Sensitive & Portable	Cr^{3+}	[53]
AuNPs	PMMA Microfluidic Chip	1.00–35.00 μM	0.33 μM	Solid-Phase Support and Phase Transition	—	Cr^{3+}	[54]
Chl-AgNPs	Chlorophyll	2–100 μM	0.62 μM	Physical Assistance & Green synthesis strategies	—	Cr^{6+}	[55]
AuNPs	PVP (Plasma synthesis)	0.1–3.0 μM	0.072 μM	Physical Assistance	—	Cr^{6+}	[56]

 doi:10.20944/preprints202601.1310.v1

				and Post-Treatment			
AuNPs	DPC	—	0.3 μM	Smart Readout & Special Response Mechanisms		Cr^{6+}	[57]
AuNPs/AgNPs	Citrate / Na	0.96–961 μM (0.05–50 ppm)	0.44 μM	Special Response Mechanisms	Wide linear range	Cr^{6+}	[58]

Mercury ions (Hg^{2+}), as highly toxic heavy metal contaminants, present significant risks to ecological systems and human health, making their trace detection very important. The fundamental recognition process of colorimetric sensing for Hg^{2+} predominantly follows the "reduction-amalgamation-aggregation" principle. Esquivel Rincón et al. [59] introduced a physical synthesis approach utilizing Laser Ablation Synthesis in Solution (LASiS), successfully avoiding surface contamination from chemical reducing agent residues present in conventional procedures. The team effectively synthesized high-purity AgNPs exhibiting a face-centered cubic (FCC) structure and clarified a distinctive "reduction-amalgamation-aggregation" sensing mechanism: Hg^{2+} is initially reduced to Hg^0 with the aid of sodium citrate, subsequently permeating the AgNP lattice to create an Ag/Hg amalgam. STEM elemental mapping verified the spatial co-localization of Ag and Hg, whereas a slight alteration in Zeta potential (from -27.12 mV to -25.31 mV) resulted in considerable particle aggregation (particle size rose to 167 nm). This system demonstrated a significant reduction in LSPR peak strength at 400 nm, accompanied by a wavelength blueshift, resulting in a visual change from bright yellow to colorless, with a detection limit of 0.2 ppm.

Biomass-mediated synthesis methodologies have attracted considerable interest owing to their cost-effectiveness and ecological sustainability; nevertheless, the disparate redox potentials of various extracts markedly affect the sensing processes. Tewari et al. [60] employed tannin-rich Diospyros kaki leaf extract to synthesize AgNPs. Their postulated mechanism suggested that the nanoscale size effect diminished the redox potential of the AgNPs, facilitating the reduction and deposition of Hg^{2+} to create an amalgam, which led to an LSPR blueshift and fluorescence quenching. This probe exhibited exceptional sensitivity (LOD 0.1 ppb) and an extensive linear range (0.1–100,000 ppb), and was effectively utilized for fluorescence imaging of liver tissue cells and pathogen suppression owing to its superior biocompatibility. Conversely, Thepwat and Kosolwattana [61] utilized carboxymethyl cellulose (CMC) derived from water hyacinth as a bifunctional compound. Due to the disparity in standard potentials (Hg^{2+}/Hg^0 +0.85 V versus Ag^+/Ag^0 +0.80 V), Hg^{2+} oxidized the surface Ag^0 of the AgNPs while undergoing reduction to create an amalgam. This method eradicated electrostatic repulsion, resulting in a substantial increase in Zeta potential from -26.2 mV to -5.89 mV, hence inducing significant aggregation. Despite its detection limit of 3.14 μM being marginally greater than that documented by Tewari, the probe exhibited remarkable anti-interference properties in complex aqueous matrices (e.g., containing Ca^{2+}, Mg^{2+}) and displayed a robust linear correlation within the concentration range of 5–45 μM. Mume et al. [62] further developed this strategy employing Salvia tiliifolia extract, attaining highly sensitive detection of Hg^{2+} (LOD 0.27 nM, linear range 0.1–100 μM) through a comparable amalgamation-induced irregular aggregation mechanism, which was effectively utilized for the analysis of tuna and environmental water samples.

To tackle the problem of signal instability resulting from conventional LSPR peak shifts during significant aggregation, Ghosh and Mondal [63] introduced an innovative spectral quantification method. In a system employing garlic extract for AgNP production, ascorbic acid was supplied to modify the particle surface state, and it was suggested to monitor the alteration in "Absorption

 doi:10.20944/preprints202601.1310.v1

Minima" in the UV region instead of the conventional LSPR peak location. This approach successfully mitigated the signal non-linearity induced by substantial aggregation during the Hg^{2+} redox process, thereby markedly improving the precision of quantitative analysis. This device exhibited the capability for multi-ion detection by successfully identifying Cd^{2+} using a functional group coordination mechanism.

In addition to the previously indicated physicochemical methods, employing the particular coordination of nucleic acids constitutes another essential strategy. Ulloa-Gomez et al. [64] created a dual-mode aptasensor that combines microfluidic paper-based analytical devices (μ-PADs) with miniature printed circuit boards (PCBs) for swift on-site trace detection. The sensing process predominantly depends on the establishment of the particular T-Hg^{2+}-T mismatch structure. Figure 5g illustrates that this method facilitates signal transmission through a salt-mediated aggregation process. Stability assessments validated that the incorporation of ssDNA aptamers proficiently protected the electric double layer of the nanoparticles from compression due to elevated ionic strength, thereby preserving probe dispersion in saline solutions (Figure 5a-b, d-e); however, the presence of Hg^{2+} induced the aptamer to adopt a rigid duplex conformation and dissociate from the particle surface, consequently eliciting an aggregation response. The alteration in microscopic state within the colorimetric module led to a notable shift or intensity reduction of the LSPR absorption peak (Figure 5c, f), resulting in a discernible color change. Concerning analytical performance, the Ps-AgNPs-based colorimetric system attained a linear detection range of 0.5–20 ppm with a LOD of 0.5 ppm, whereas the Ps-AuNPs variant was mostly utilized for qualitative screening (LOD 5 ppm). The electrochemical module demonstrated superior sensitivity, achieving a limit of detection of 0.01 ppm.

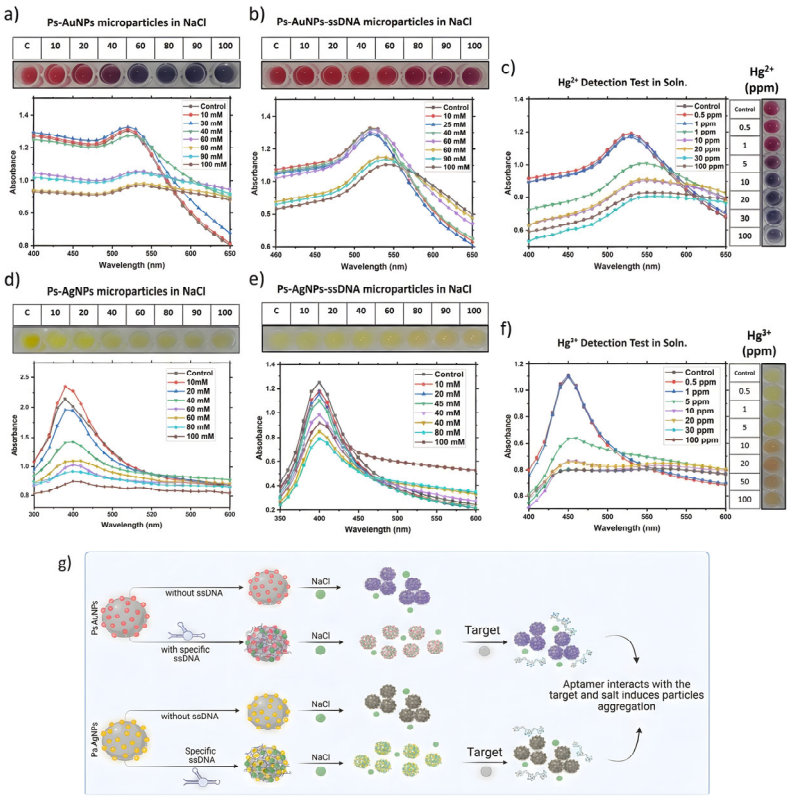

Figure 5. Evaluation of stability and colorimetric sensing efficacy of the aptamer-functionalized microparticles [64].

Yang et al. [65] devised a label-free colorimetric sensing approach utilizing a DNA-mediated charge neutralization mechanism of AuNPs, aimed at the on-site detection of Hg^{2+} in environmental

 doi:10.20944/preprints202601.1310.v1

water and cosmetics. This research developed a "probe-blocker" double-stranded DNA system consisting of probe DNA (p-DNA) and blocker DNA (b-DNA). The sensing mechanism utilizes the strong affinity of T-Hg^{2+}-T specific mismatched base pairs: in the presence of the target Hg^{2+}, the replacement DNA (r-DNA) preferentially associates with the p-DNA, resulting in the release of the long-chain b-DNA from the double-stranded configuration. The free b-DNA, owing to its extended chain length, efficiently adsorbs onto the AuNP surface, thereby markedly impeding Thioflavin T (ThT)-induced charge neutralization and aggregation of the AuNPs. This approach accomplished visual detection of Hg^{2+} using smartphone image analysis of the chromaticity alteration of the AuNP solution from blue (aggregated state) to red (dispersed state), without necessitating supplementary enzymatic aid or signal amplification procedures. Experimental data indicated that this approach had a linear response range for Hg^{2+} of 0.005–1 μM, with a LOD of 2.85 nM. This sensor platform integrates portable smartphone data gathering technology, offering a cost-effective, high-precision analytical instrument for the swift on-site detection of detectable mercury contamination in the environment and daily consumer products.

To overcome the restrictions of high cost and sensitivity to deactivation associated with biological macromolecules, Liu et al. [66] broadened the sensing application of pharmaceutical small molecules by building a ribavirin-functionalized gold nanoparticle probe (Rib-AuNPs). This method employs electrostatic interactions to attach positively charged ribavirin to the surface of negatively charged AuNPs. DFT theoretical simulations and Electrostatic Potential (ESP) research demonstrated that the triazole nitrogen atoms and amide group oxygen atoms on the ribavirin surface function as highly reactive sites, capable of establishing a stable "chelating-bridging" structure with Hg^{2+}. This particular coordination diminishes the electrostatic repulsion among nanoparticles (Zeta potential reduced from -31.7 mV to -18.2 mV), prompting a notable aggregation transition of AuNPs from wine-red to gray-blue (LSPR peak redshifted from 520 nm to 654 nm). This sensor exhibited remarkable anti-interference capability in intricate matrices like tap water and lake water (withstanding 16 competing ions) and accomplished segmented detection across an extensive linear range. The UV-vis spectral limit of detection was 3.64 nM, while the naked-eye visual detection limit was 0.20 mM, offering a quick and highly selective analytical instrument for environmental water monitoring.

The trace accumulation of lead ions (Pb^{2+}), a non-essential and highly neurotoxic heavy metal, in environmental water bodies poses a severe challenge to public health. In the realm of green synthesis of nanomaterials,Do Dat et al. [67] generated AuNPs via a one-step approach utilizing Andrographis paniculata leaf extract. Their analysis demonstrated that the phenolic hydroxyl and carbonyl groups within the extract functioned as both stabilizing agents and recognition sites; the injection of Pb^{2+} upset the surface electrostatic equilibrium and promoted fast particle aggregation. This probe displayed a strong response to Pb^{2+} within a linear range of 0–100 μM (LOD 12.661 μM) while displaying “multifunctional” potential for the catalytic degradation of organic dyes and bacteriostasis. To further boost detection sensitivity, Zannotti et al. [68] undertook an in-depth analysis into the AuNPs@OPE system synthesized from orange peel extract (OPE), specifically explaining the regulatory function of reaction kinetics on sensitivity. By prolonging the reaction time to enhance the coordination-driven aggregation effect, the system reached a linear range of 0.8–9.9 μM with a LOD as low as 0.05 μM, fulfilling WHO criteria for drinking water. Addressing the difficulty of multi-ion interference in complicated matrices, the researchers introduced chemometric approaches in a subsequent study on AgNPs@OPE [69]. By combining Principal Component Analysis (PCA) and Linear Discriminant Analysis (LDA), they efficiently resolved the spectrum overlap between Pb^{2+} and Cd^{2+} (accuracy 98.5%). Hladun et al. [70] built a universal colorimetric probe utilizing ascorbic acid based on the complexation mechanism between metal ions and hydroxyl groups, achieving simultaneous detection of Pb^{2+} (LOD 5.4 ppb) and Cr^{6+}.

The implementation of highly specific biological enzymes signifies an additional method for enhancing quantitative precision. Yan et al. [71] deviated from the traditional “metal-ion-induced direct aggregation” model by developing a Pb^{2+} sensor utilizing DNAzyme cleavage. In this system,

 doi:10.20944/preprints202601.1310.v1

Pb^{2+} functions as a cofactor to activate the DNAzyme, facilitating the cleavage of the substrate strand and resulting in the disruption of single-stranded DNA modified on the AuNP surface, thus preserving the dispersed state of the AuNPs (red); conversely, in the absence of Pb^{2+}, salt-induced aggregation transpires (blue). This technique adeptly transforms the alteration in dispersion state into a dual-modal signal (Figure 6A): fluorescence quenching of carbon quantum dots (CDs) by scattered AuNPs (FRET mechanism) and fluctuations in the Tyndall scattering effect induced by aggregates. This dual-channel technique enabled ultrasensitive detection of Pb^{2+}, exhibiting a colorimetric linear range of 2.4×10^{-14} to 8.0×10^{-10} mol/L and a LOD as low as 0.11 pM, underscoring its significant practical utility in complicated food matrices, including preserved eggs (Figure 6B).

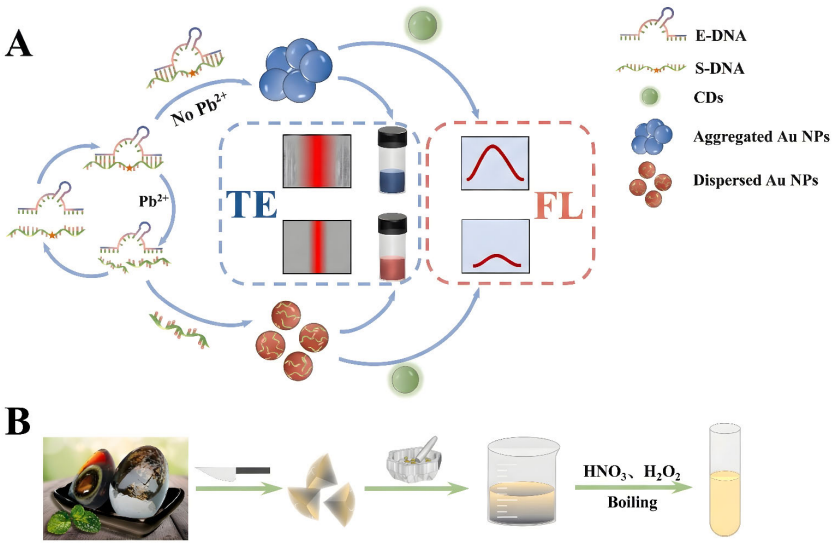

Figure 6. Schematic representation of the DNAzyme-mediated dual-modal sensing approach for Pb^{2+} [71].

Despite the advancements in enzymatic cleavage strategies that have significantly enhanced sensitivity, DNAzyme-AuNP systems frequently face a limitation of sluggish dissociation kinetics in practical applications, attributable to the excessive stability of the fully matched duplex structure, which restricts the signal response rate. Liu et al. [72] introduced a "mismatch acceleration" technique to tackle this thermodynamic and kinetic problem. The incorporation of A-C mismatch base pairs into the substrate strand greatly diminished duplex stability (lower T_m), hence significantly expediting the Pb^{2+}-induced aggregation breakdown and redispersion process while preserving specificity. This approach attained a rapid response through mismatch sequence optimization within a linear range of 10–300 nM, with a detection limit of 8.6 nM.

Nkanyezi Penuel Kubheka et al. [73] developed a cost-effective quantitative method utilizing ImageJ image processing software to mitigate the reliance of traditional colorimetry on analytical instrumentation. The approach reached a limit of detection of 0.01 mg/L within a linear range of 0.1–20 mg/L by employing the color transition caused by Pb^{2+}-mediated AuNP aggregation alongside smartphone RGB analysis, demonstrating performance akin to that of complicated customized probes.

Moreover, concerning the detection of the heavy metal cadmium (Cd^{2+}) in cosmetics, He et al. [74] suggested a sensing approach employing unmodified AuNPs modulated by the cationic dye SYBR Green I and a particular aptamer. This process utilizes the strong attraction between Cd^{2+} and the aptamer to cause the desorption of the aptamer from the AuNP surface. As a result, the unshielded nanoparticles experience charge neutralization and significant aggregation due to electrostatic interactions with the dye, resulting in a LOD of 0.27 μM and a linear detection range of 0.2–4 μM. Munazza Arain et al. [75] advanced the approach of small-molecule functionalization by synthesizing Secnidazole-modified AgNP probes in a single step. This system utilizes the

 doi:10.20944/preprints202601.1310.v1

pronounced affinity of Cd^{2+} for the hydroxyl groups of surface ligands to facilitate ligand desorption and subsequent nanoparticle aggregation, attaining a low LOD of 0.021 μM within a linear range of 5–27 μM, and was effectively employed for detection in complex biological samples, including plasma.

Table 2. Analytical efficacy of colorimetric tests for the identification of mercury (Hg^{2+}) and lead (Pb^{2+}) ions.

Nanostructure	Ligand	Linear Range	LOD	Method	Evaluation	Ion	Ref.
AgNPs	Citrate (Laser Ablation)	—	1.0 μM (0.2 ppm)	Physical Assistance and Post-Treatment	—	Hg^{2+}	[59]
AgNPs	*Diospyros kaki* extract	0.5 nM–500 μM (0.1–100,000 ppb)	0.5 nM (0.1 ppb)	Green synthesis strategies	Wide linear range	Hg^{2+}	[60]
AgNPs	CMC (*Water hyacinth*)	5–45 μM	3.14 μM	Green synthesis strategies	—	Hg^{2+}	[61]
AgNPs	*Salvia tiliifolia* extract	0.1–100 μM	0.27 nM	Green synthesis strategies	Ultrasensitive	Hg^{2+}	[62]
Ps-AgNPs	DNA Aptamer	2.5–100 μM (0.5–20 ppm)	2.5 μM (0.5 ppm)	Solid-Phase Support & Multimodal sensing	Sensitive & Portable	Hg^{2+}	[64]
AuNPs	DNA (Probe-blocker)	0.005–1 μM	2.85 nM	Ligand Engineering & Smart Readout	Sensitive & Portable	Hg^{2+}	[65]
Rib-AuNPs	Ribavirin	—	3.64 nM	Ligand Engineering	—	Hg^{2+}	[66]
AuNPs	*Andrographis paniculata* extract	0–100 μM	12.661 μM	Green synthesis strategies	—	Pb^{2+}	[67]
AuNPs	Orange peel extract (OPE)	0.8–9.9 μM	0.05 μM	Green synthesis strategies & Special Response Mechanisms	—	Pb^{2+}	[68]
AuNPs & CDs	DNAzyme	2.4×10^{-14}–8.0×10^{-10} M	0.11 pM	Ligand Engineering & Multimodal sensing	Ultrasensitive	Pb^{2+}	[71]
AuNPs	DNAzyme (Mismatch)	10–300 nM	8.6 nM	Special Response Mechanisms	—	Pb^{2+}	[72]

 doi:10.20944/preprints202601.1310.v1

AuNPs	Unmodified	0.48–96.5 μM (0.1–20 mg/L)	48 nM (0.01 mg/L)	Smart Readout and Algorithmic Enhancement	Sensitive & Portable	Pb^{2+}	[73]

3.2. Transition Metal Ions

This section addresses the colorimetric detection of iron (Fe), nickel (Ni), and copper (Cu) ions. Iron ions mostly occur in divalent (Fe^{2+}) and trivalent (Fe^{3+}) oxidation states in biological and environmental contexts, with the choice of surface ligands being crucial for differentiating between these valences.Dayanidhi et al. [76] illustrated the capability of employing saponins from Sapindus mukorossi extract as reducing agents and recognition ligands for valence-specific recognition. The research uncovered a distinct mechanism involving ligand-to-metal charge transfer (LMCT): oxygen atoms with high-energy lone pair electrons in the saponin backbone engage with Fe^{2+} or Fe^{3+} that have low-energy unoccupied $3d^0$ orbitals. This interaction produced unique spectral responses: Fe^{2+} increased the SPR band intensity and altered the solution color to black, whereas Fe^{3+} diminished the SPR band and transformed the solution to white. The probe effectively attained precise distinction between Fe^{2+} (LOD 1 μM) and Fe^{3+} (LOD 5 μM), exhibiting a linear detection range of 0–100 μM for both ions.

To further address the challenges of portability and non-specific aggregation associated with liquid-phase probes in practical applications, Andreani et al. [77] proposed a gel matrix confinement strategy (Figure 7). They synthesized AuNPs using α-cyclodextrin and β-cyclodextrin as stabilizers and integrated them into an agarose gel matrix. The cavity structure of the CDs and the gel network synergistically prevented non-specific aggregation, while the addition of Fe^{3+} induced the controlled aggregation of AuNPs, resulting in a color transition of the gel from pink to purple (Figure 7, top panel). In particular, the sensor based on β-CDs, benefiting from superior stabilizing capability and smaller particle size (~17.13 nm), demonstrated excellent performance (LOD 0.20 mg/L, linear range 2–18 mg/L).

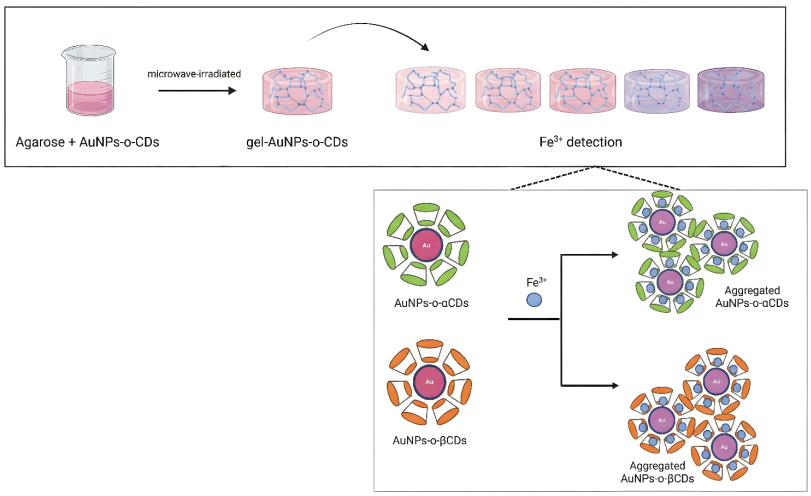

Figure 7. Schematic representation of the fabrication process for gel-based AuNPs sensors and the colorimetric detection technique for Fe^{3+} [77].

The principal obstacle in the colorimetric detection of nickel ions (Ni^{2+}) is the efficient removal of interference from concurrent divalent ions. Enhancing surface ligand chemistry alongside digital image colorimetry (DIC) can markedly improve the specificity and precision of Ni^{2+} detection.Patra et al. [78] utilized green tea extract for the eco-friendly synthesis of AuNPs, employing rich polyphenols, including gallocatechin and epicatechin gallate, as functional capping agents. The

 doi:10.20944/preprints202601.1310.v1

hydroxyl (–OH) and carbonyl (C=O) functional groups on these biomolecules provide several coordination sites for Ni^{2+}, facilitating electrostatic attraction and coordination binding between the positively charged Ni^{2+} and the negatively charged AuNP surface. This interaction caused a red shift in LSPR absorption peak from 528 nm to 556 nm, along with a color change of the solution from pink to purple (Figure 8a–b). The probe demonstrated exceptional anti-interference capability regarding Ni^{2+} (Figure 8d), exhibiting a robust linear response within the range of 0.001–1 mg/L (Figure 8c) and achieving a LOD as low as 0.001 mg/L, surpassing World Health Organization (WHO) standards, thereby validating the effectiveness of natural polyphenol ligands in the specific recognition of Ni^{2+}.

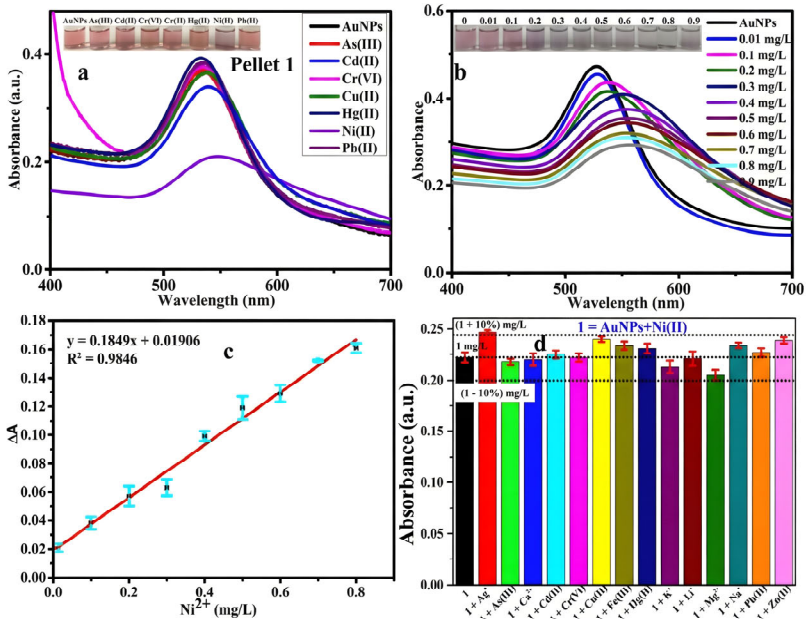

Figure 8. Colorimetric sensing efficacy of the bio-synthesized AuNPs for Ni^{2+} [78].

Nubatonis et al. [79] devised a detection strategy utilizing chemical ligand-functionalized AgNPs integrated with smartphone-based DIC analysis through digital analytic techniques. Unlike intricate biological extracts, they employed mercaptosuccinic acid (MSA) and ethylenediaminetetraacetic acid (EDTA) to alter AgNPs. They facilitated AgNP aggregation by utilizing the particular binding sites of carboxyl, amino, and thiol groups through robust metal-ligand coordination. This induced a color transition in the solution from yellow to blue and a notable shift in the LSPR peak from 402 nm to 620 nm. This method attained a LOD of 3.57 μM and a linear detection range of 10–300 μM by transforming image RGB values into Euclidean distances for quantitative analysis. This research illustrates that the integration of meticulously designed chemical ligands with sophisticated imaging algorithms significantly improves the accuracy of on-site detection of transition metal ions.

Wu et al. [80] devised a green, ligand-free gold nanoparticle probe for the detection of copper ions (Cu^{2+}). Polysaccharides and proteins from the alga Padina australis chelated with Cu^{2+} through their $–NH_2$ and –OH groups, causing the aggregation of AuNPs and leading to a notable red shift (from 520 nm to 630 nm). This technique is straightforward and effective, exhibiting commendable linearity for the quantitative measurement of Cu^{2+} within the range of 20–60 μM, with a LOD of 0.43 μM. Likewise, Aqillah et al. [81] employed the traditional citrate reduction technique to synthesis AuNPs, utilizing a detection methodology predicated on Cu^{2+}-induced aggregation through citrate displacement or bridging. Their research concentrated on enhancing a smartphone-based digital image colorimetry (DIC) readout system, attaining accuracy that surpasses conventional UV-Vis spectroscopy by analyzing the blue channel.

 doi:10.20944/preprints202601.1310.v1

Nguyen and colleagues [82] proposed an approach for in situ hydrogel synthesis. They utilized L-cysteine to decrease $HAuCl_4$ within an agar hydrogel matrix. In contrast to liquid-phase environments, the agar hydrogel functioned as a dynamic regulator of molecular diffusion, offering structural support while simultaneously improving dispersion stability by limiting the Brownian motion of the AuNPs. Cu^{2+} acted as a cross-linker, interacting with the functional groups (–SH, –COOH, $–NH_2$) of L-cysteine to promote aggregation. This method attained a LOD of 0.65 μM and a linear range of 10 to 70 μM. This "matrix-assisted" approach substantially mitigated the problem of spontaneous aggregation frequently encountered in conventional colloidal probes (solidification of liquid-phase probes).

Colford and Dhirani [83] presented a novel "pH-selective precipitation (PSP)" purification process to address the influence of surface ligand purity on sensitivity. They indicated that remaining excess capping agents from conventional production can competitively bind metal ions, thus reducing sensor sensitivity. The researchers generated mercaptobenzoic acid (MBA)-functionalized AuNPs and utilized the PSP technique, adjusting pH to facilitate reversible aggregation and redispersion for the removal of excess citrate and MBA (Figure 9). The purified probes (MBA-AuNPs) demonstrated remarkable sensitivity to Cu^{2+}, as the particular chelation between Cu^{2+} and carboxyl groups prompted the formation of aggregates (Figure 9, step 6). This approach boosted the LOD by 100-fold (achieving 10^{-5} M) compared to unpurified probes, and the direct coordination of Cu^{2+} to the MBA monolayer was verified using X-ray photoelectron spectroscopy (XPS) and SERS. This discovery highlights the essential importance of ligand layer purification in the development of ultrasensitive colorimetric sensors.

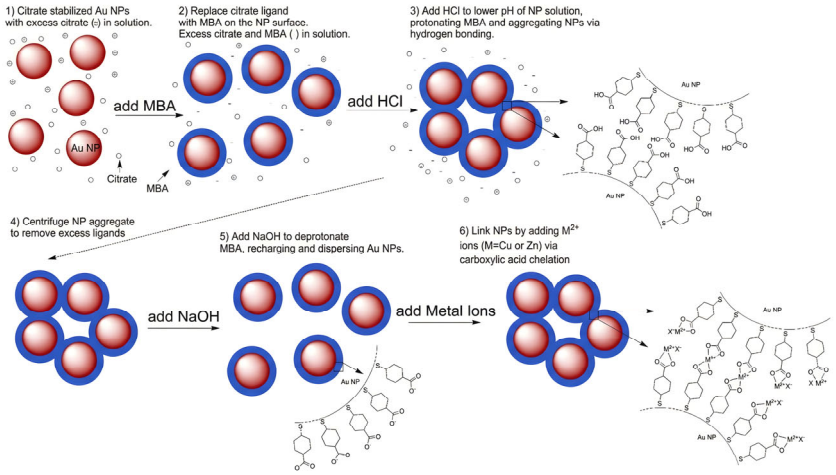

Figure 9. Schematic illustration of the ligand exchange and pH-selective precipitation (PSP) purification method.

Table 3. Analytical efficacy of colorimetric tests for the identification of iron (Fe), nickel (Ni^{2+}), and copper (Cu^{2+}) ions.

Nanostructure	Ligand	Linear Range	LOD	Method	Evaluation	Ion	Ref.
Ag/Au NPs	Saponins	0–100 μM	1 μM	Green synthesis strategies & Special Response Mechanisms	—	$Fe^{2+/3+}$	[76]

 doi:10.20944/preprints202601.1310.v1

AuNPs	Cyclodextrin (Gel matrix)	35.8–322 μM (2–18 mg/L)	3.6 μM (0.20 mg/L)	Solid-Phase Support and Phase Transition	—	Fe^{3+}	[77]
AuNPs	Green tea extract	17 nM–17 μM (0.001–1 mg/L)	17 nM (0.001 mg/L)	Green synthesis & Smart Readout		Ni^{2+}	[78]
AgNPs	MSA & EDTA	10–300 μM	3.57 μM	Ligand Engineering & Smart Readout	Sensitive & Portable	Ni^{2+}	[79]
AuNPs	*Padina australis* polysaccharides	20–60 μM	0.43 μM	Green synthesis strategies	—	Cu^{2+}	[80]
AuNPs	L-Cysteine (Hydrogel)	10–70 μM	0.65 μM	Solid-Phase Support and Phase Transition	—	Cu^{2+}	[82]
AuNPs	MBA (Purified)	—	10 μM	Physical Assistance and Post-Treatment	—	Cu^{2+}	[83]

3.3. Other Metal Ions

This section addresses the colorimetric detection of aluminum (Al^{3+}) and various metal ions. A major technique for attaining selective recognition of Al^{3+} includes altering noble metal nanoparticles with natural or synthesized small molecules rich in oxygen and nitrogen donors, which induce aggregation via metal-ligand interactions. Joshi et al. [84], Rastogi et al. [85], and Ghodake et al. [86] utilized indole-2-carboxylic acid, ascorbic acid, and gallic acid as functional ligands, respectively, to construct extremely sensitive silver/gold nanoprobes. The limits of detection (LOD) were 0.01 ppm, 12.5 ppb, and 1.48 μM, respectively, with Refs. [84] and [85] reporting linear ranges of 0.5–10 ppm and 100–350 ppb, respectively. Building on this foundation, important innovations have further increased detecting functionalities:Bezuneh et al. [87] introduced a competitive coordination mechanism using tannic acid-functionalized AgNPs, achieving dual detection of Al^{3+} (LOD 0.2 μM, linear range 2–25 μM) and F^-; meanwhile, Montenegro et al. [88] modified AgNPs with carbon dots and combined them with chemometric modeling (MCR-ALS) to quantitatively resolve the binding kinetics of Al^{3+} (LOD 3.5 μM).

Taheri and Khayatian [89] developed an economical microfluidic chip utilizing poly(methyl methacrylate) (PMMA) and cotton thread for on-site portable detection. This research utilized ammonium pyrrolidine-1-carbodithioate (APDC) to alter AgNPs, leveraging the particular interaction between the nitrogen and sulfur atoms in APDC and the metal ions to promote aggregation, thus facilitating concurrent colorimetric detection of Al^{3+} and Cr^{3+}. The introduction of NaF as a masking agent effectively mitigated interference from concurrent ions. The limits of detection for Al^{3+} and Cr^{3+} were 3.55 nM and 10.66 nM, respectively, with linear detection ranges of 0.01–250 μM and 0.1–220 μM, respectively, confirming the applicability of microfluidic technology in multi-component environmental study.

In relation to the essential technological component tellurium (Te^{4+}), Kim et al. [90] employed natural alginate as a bifunctional agent for the environmentally friendly synthesis of AgNPs. Based on the chelation of Te^{4+} with surface carboxyl/hydroxyl groups inducing ligand dissociation and

 doi:10.20944/preprints202601.1310.v1

particle aggregation, this method effectively shielded interference from congeneric elements (As, Se), achieving a LOD of 22 nM and a linear response range of 31.3–407.5 nM, validating its applicability in environmental water analysis. For the detection of the rare earth element La^{3+}, Hussain et al. [91] developed a smartphone-based paper sensing platform utilizing resorcinarene-modified AgNPs. Relying on an aggregation mechanism generated by the particular coordination of La^{3+} with macrocyclic oxygen atoms, colorimetric identification from yellow to gray was obtained. This approach revealed a good linear response to La^{3+} in the range of 0.05–100 μM, with a LOD of 15 nM.

The colorimetric detection of alkali metal ions fundamentally depends on electric double layer compression and the alteration of colloidal stability. Hsiao et al. [92] examined the influence of AuNP surface potential on the sensitivity of Na^+ detection. The research indicated that the Zeta potential of AuNPs rose from -87.7 mV to -58.2 mV following treatment with ascorbic acid, resulting in a metastable condition. The addition of Na^+ diminished the activation energy for aggregation, measured at 22.5 $kJ \cdot mol^{-1}$, in accordance with the ionic strength-induced aggregation outlined by DLVO theory. This probe accomplished visual detection of Na^+ (LOD around 30 mM) via straightforward electrostatic interactions, and a second-order polynomial regression model was developed for quantitative analysis, offering a cost-effective approach for high-concentration salt detection.Berasarte et al. [93] established a universal electrolyte detection platform for Na^+, K^+, Ca^{2+}, and Mg^{2+} via lysine-assisted AgNP aggregation. Lysine served as a crucial inducer, facilitating AgNP aggregation and color alteration in the presence of electrolytes. This study's novelty resides in the thorough integration of digital image analysis (DIA) technologies, utilizing principal component analysis (PCA) for particle optimization and partial least squares (PLS) models to mitigate K^+ interference on Na^+, ensuring a relative inaccuracy of no more than 13%. This technique, which integrates multivariate calibration with smartphone imaging, signifies an advancement of colorimetric sensors towards enhanced portability and intelligence.

Patel et al. [94] introduced a morphology-regulated "multicolor" sensing method, employing bovine serum albumin (BSA) as a bifunctional reagent to produce silver nanostructures with varying aspect ratios and starting hues (yellow, orange, green, blue). This study demonstrated that the ion response of the probes exhibits considerable "shape dependence": heavy metal ions (Cr^{3+}, Hg^{2+}) predominantly induce characteristic red-shifted aggregation of spherical particles (yellow/orange) through coordination with surface amino or carboxyl groups of BSA; conversely, the alkali metal K^+, which is challenging to complex, specifically destabilizes plate-like nanostructures (green/blue) and induces a blue shift (hypsochromic shift) in the absorption spectra, thereby facilitating visual differentiation of multiple ions in complex matrices based on distinct spectral evolution patterns.

4. SERS Sensors

The aggregation of nanoparticles causes significant alterations in the LSPR spectrum and concurrently activates robust electromagnetic coupling effects at the microscopic level. SERS detection principally utilizes the high-density electromagnetic "hotspots" created within the interparticle gaps of aggregates to exponentially enhance the signals of molecules situated in these areas. This technology allows for the dynamic modulation of local enhancement factors by changing the assembly or disassembly state of nanoparticles through target ions, facilitating quantitative study of targets based on "Signal-on" or "Signal-off" Raman mechanisms.

4.1. Heavy Metal Ions

Lead ions (Pb^{2+}) exhibit considerable biological toxicity and can engage in robust interactions with sulfur- and nitrogen-containing groups in animals. Their accumulation in environmental and biological systems presents significant hazards to the nervous system. The coordination interaction between Pb^{2+} and surface-modified ligands to promote nanoparticle aggregation is a crucial method for manufacturing SERS probes.Frost et al. [95] devised an efficient SERS sensing device utilizing citrate-functionalized AuNPs. This study utilized citrate molecules as dual-functional agents serving as colloidal stabilizers and identification probes. Upon the introduction of Pb^{2+}, it exhibits robust

 doi:10.20944/preprints202601.1310.v1

coordination with the carboxyl (COO^-) and hydroxyl (OH) groups on the citrate surface, resulting in the aggregation of 6 nm AuNPs. This leads to a redshift and broadening of the LSPR absorption band. The aggregation process creates efficient SERS hotspots, resulting in a significant reduction of the citrate v(O-H) vibrational peak strength (about 3200 cm^{-1}) as Pb^{2+} concentration increases. The approach demonstrates a linear response range of 50–1000 ng/L and a LOD of 25 ng/L, and it has been effectively utilized for fast detection in aqueous environmental systems.

Xu et al. [96] developed a sensing platform utilizing L-cysteine (L-cys) functionalized Au@Ag core-shell nanoparticles (Au@Ag NPs). In contrast to monometallic AuNPs, the Au@Ag NPs merge the stability of the gold core with the enhanced dielectric characteristics of the silver shell, exhibiting superior localized electromagnetic field enhancement capabilities. In this system, Pb^{2+} selectively chelates with the carboxyl and amino groups of L-cysteine, causing the Au@Ag nanoparticles to shift from a dispersed to an aggregated form, resulting in a substantial amplification of the Raman signal of the reporter molecule, 4-aminothiophenol (4-ATP). The assembly process is clearly validated by transmission electron microscopy (TEM) pictures and dynamic light scattering (DLS) data, as illustrated in Figure 10. The creation of the Au@Ag core-shell structure results in a significant increase in hydrodynamic diameter; subsequent injection of Pb^{2+} causes the nanoparticles to shift from a monodisperse state to separate agglomerates (Figure 10F), resulting in a substantial rise in average particle size. These nanoscale aggregates offer numerous electromagnetic hotspots for SERS signal amplification. This method efficiently mitigates interference from ions such as Hg^{2+} by employing potassium thiocyanate (KSCN) as a masking agent, resulting in a low LOD of 1 pM and a logarithmic linear standard curve spanning from 5 pM to 10 nM. The sensitivity has been enhanced by 3 to 4 orders of magnitude relative to conventional colorimetric techniques.

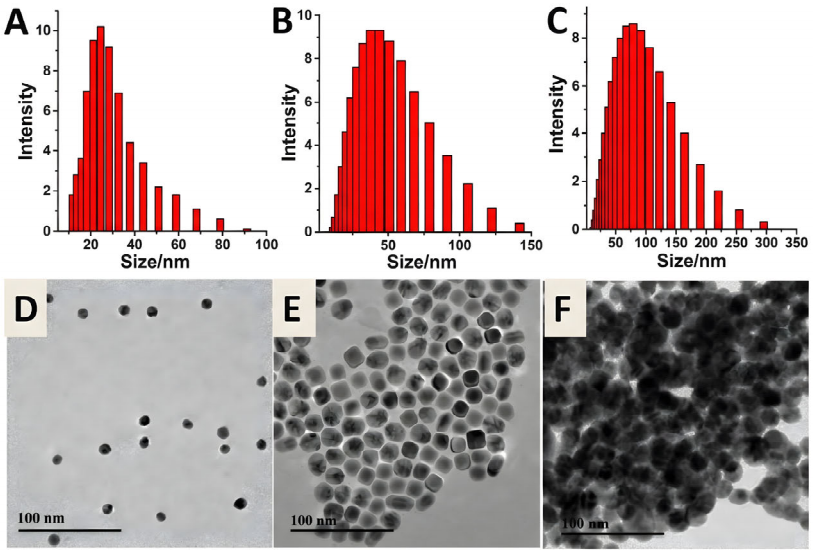

Figure 10. Characterization of the structural evolution and Pb^{2+}-induced aggregation of the sensing probe [96].

Anisotropic nanomaterials can produce more potent electromagnetic field enhancement effects at their tips owing to their geometric configurations. Liu et al. [97] engineered gold-core silver-shell nanorods (Au@Ag NRs) co-modified with GSH and 4-MBA. GSH is tethered through Ag-S interactions, and its accessible carboxyl groups, in conjunction with 4-MBA, function as binding sites for Pb^{2+}. The introduction of Pb^{2+} promotes the self-assembly and aggregation of the nanorods, resulting in the formation of high-density hotspots in the interparticle spaces, which markedly amplifies the distinctive peak of 4-MBA at 1072 cm^{-1}. This probe has a LOD of 0.021 μg/L and a linear range of 0.5 to 1000 μg/L. The method's suitability for on-site food safety screening was validated through testing in intricate food matrices, including tea powder and sticky rice flour.

 doi:10.20944/preprints202601.1310.v1

Strategies for DNAzyme functionalization employ specialized catalytic cleavage reactions activated by metal ions to accurately control the surface properties and aggregation behavior of nanoparticles, hence enhancing detection selectivity considerably. Liu et al. [98] introduced a SERRS sensing system that integrates DNAzyme with Au/Ag NPs. This approach utilizes the catalytic activity of Pb^{2+} to cleave the substrate DNA strand, in contrast to the previously reported small-molecule ligand-induced aggregation. In the presence of Pb^{2+}, the cleaved single-stranded DNA adheres to the nanoparticle surface, resulting in the development of "loose aggregates" of Au/Ag NPs with elevated SERRS activity, thereby markedly amplifying the signal of Rhodamine 6G (RhG). In the absence of Pb^{2+}, the undamaged double-stranded DNA fails to offer adequate protection, resulting in tight aggregation of the system and yielding only a faint background signal. This technique adeptly utilizes the specificity of DNAzyme, attaining a limit of detection of 7×10^{-9} M and a linear detection range of 5.0×10^{-8} to 6.0×10^{-7} mol/L, while exhibiting remarkable anti-interference properties.

The colorimetric-SERS dual-mode detection method integrates the benefits of macroscopic color alterations with microscopic spectrum examination, facilitating the differentiated identification of several components through unique surface binding mechanisms. Chadha et al. [99] created a 2-thiazoline-2-thiol (TT) functionalized AuNPs sensor, enabling the differential detection of Pb^{2+} and Hg^{2+} by dual-mode analysis. Both Pb^{2+} and Hg^{2+} can induce the aggregation of AuNPs and result in a colorimetric shift (redshift) in the solution; however, their microscopic surface mechanisms differ: Hg^{2+} promotes aggregation and establishes stable $Hg(TT)_2$ complexes on the gold surface, leveraging the hotspot effect for SERS signal enhancement (Signal-on), whereas Pb^{2+}, while also inducing aggregation, forms $Pb(TT)_2$ complexes with a weaker affinity for the gold surface, resulting in desorption and subsequent SERS signal quenching (Signal-off). The investigation via X-ray photoelectron spectroscopy (XPS) validated this competitive adsorption mechanism. Experimental results demonstrated a strong linear correlation between variations in SERS relative intensity and ion concentration within the range of 0.1 to 10 μM. The approach attained a LOD of 0.409 μM (about 0.111 ppm) for Hg^{2+} and 0.344 μM (approximately 0.096 ppm) for Pb^{2+}, satisfying the sensitivity criteria for routine environmental monitoring.

Wang et al. [100] were pioneers in developing a sensing system for AgNPs using T-rich aptamers. Utilizing the notion that Hg^{2+} prompts the aptamer to fold into a T-Hg^{2+}-T configuration, thereby diminishing its protective function, the method incorporated cationic spermine to facilitate nanoparticle aggregation. This accomplished a "Signal-on" SERS detection of the surface-labeled chemical TAMRA (LOD 5 nM). While physical aggregation procedures are efficient, chemical mechanisms involving amalgam production between mercury ions and silver are more commonly utilized in SERS detection with silver-based nanomaterials. The research conducted by Hassan et al. [101] frequently illustrates this idea of non-aggregation. This work employed Au@Ag nanoparticles as substrates; in the presence of Hg^{2+}, a distinct reaction transpired with the silver shell to produce Ag-Hg amalgam. This chemical reaction modified the surface plasmon resonance characteristics of the nanoparticles and resulted in the desorption or displacement of the surface-adsorbed signal molecule (R6G), which macroscopically appeared as a substantial reduction in the SERS signal with rising Hg^{2+} concentration (Signal-off).

Table 4. Analytical efficacy of SERS tests for the identification of lead (Pb^{2+}) and mercury (Hg^{2+}) ions.

Nanostructure	Ligand	Linear Range	LOD	Method	Evaluation	Ion	Ref.
AuNPs	Citrate	0.24–4.8 nM (50–1000 ng/L)	0.12 nM (25 ng/L)	Molecular Probe Engineering	—	Pb^{2+}	[95]

 doi:10.20944/preprints202601.1310.v1

Au@Ag NPs	L-cysteine & 4-ATP	5 pM–10 nM	1 pM	Plasmonic nanohybrid design	Ultrasensitive	Pb^{2+}	[96]
Au@Ag NRs	GSH & 4-MBA	2.4 nM–4.8 μM (0.5–1000 μg/L)	0.1 nM (0.021 μg/L)	Plasmonic nanohybrid design	Wide linear range	Pb^{2+}	[97]
Au/AgNPs	DNAzyme	5.0×10^{-8}–6.0×10^{-7} M	7 nM	Special Response Mechanisms	—	Pb^{2+}	[98]
AgNPs	Aptamer / Spermine	—	5 nM	Molecular Probe Engineering	—	Hg^{2+}	[100]
AgNPs	L-cysteine	—	Cu: 10pM Hg: 1 pM	Molecular Probe Engineering	Ultrasensitive	Cu^{2+}, Hg^{2+}	[108]

Dasary et al. [102] devised an ultrasensitive detection method for cadmium ions (Cd^{2+}) utilizing multi-ligand synergistic effects. They employed Alizarin as the Raman reporter molecule and incorporated 3-mercaptopropionic acid (MPA) and 2,6-pyridinedicarboxylic acid (PDCA) to alter 13 nm AuNPs. Under conditions of pH 8.5, Cd^{2+} established a stable hexadentate coordination complex with the surface ligands, resulting in particle aggregation and eliciting substantial electromagnetic field coupling effects, which amplified the distinctive peak of Alizarin at 1335 cm^{-1} by about 10^7-fold. This approach is distinguished by its exceptional sensitivity (LOD as low as 10 ppt) and reversibility under EDTA regulation, demonstrating that the aggregation process arises from ion-template chelation. Du and Jing [103] presented a "one-pot" technique to streamline the synthesis process, employing dopamine (DA) as both a reducing and capping agent to fabricate functionalized AuNPs, thereby developing a sensor based on a "Signal-on" mechanism. The quinone moieties in the oxidation products of dopamine demonstrate selective recognition for Cd^{2+} ions. The investigation of two-dimensional correlation spectroscopy (2D-COS) verified that the robust chelation between quinone groups and Cd^{2+} prompted swift aggregation of AuNPs, leading to a substantial amplification of the Raman signal at 1618 cm^{-1}. This probe attained a detection limit of 10^{-8} M, exhibiting a linear range from 10^{-4} M to 10^{-8} M, and showcased remarkable anti-interference efficacy in intricate matrices, including copper smelting wastewater. In contrast to the direct cross-linking technique, Guo et al. [104] employed the notion of "ligand competitive displacement" to develop an R6G/GSH/AuNPs sensing platform. This technique utilized GSH as a stabilizing agent. The stability of the $[Cd(SG)_4]$ complex, produced by Cd-S and Cd-N bonds with a binding energy of 208.5 kJ/mol, is considerably greater than that of the Au-S bond, resulting in the desorption of GSH from the surface of AuNPs in the presence of Cd^{2+}. The AuNPs, having shed their protective coating, aggregated due to the presence of electrolytes, hence activating the SERS signal of Rhodamine 6G (R6G). This technique successfully circumvented non-specific adsorption problems, attaining a limit of detection of 10 ppb for Cd^{2+} within a linear range of 0.5 ppm to 20 ppm.

In the realm of SERS detection of Cr^{3+}, Ye et al. [105] developed a Tween 20-stabilized citrate-capped AuNPs system. By employing the targeted chelation of Cr^{3+} with surface citrate to mitigate steric hindrance and promote aggregation, they markedly amplified the signal of the reporter molecule (2-ATP), attaining highly selective detection within a linear range of 50–200 nM (LOD 50 nM). Ly and Joo [106] employed EDTA-modified AgNPs to demonstrate that the conformational alteration caused by the coordination of Cr^{3+} with EDTA might initiate nanoparticle aggregation. This procedure markedly amplified the metal-ligand (Cr-N) vibrational signal at 563 cm^{-1}, attaining a detection threshold of 0.5 μM in seawater matrices. Cheng et al. [107] developed Au-core/Ag-shell composite nanoprobes (17.5 nm Au core/4.7 nm Ag shell) for the quantitative assessment of Cr^{3+},

 doi:10.20944/preprints202601.1310.v1

utilizing 4-MBA as the signaling molecule and DL-mercaptosuccinic acid (DL-MSA) as the recognition component. The precise chelation of Cr^{3+} with the terminal carboxyl groups of DL-MSA facilitated the cross-linking and aggregation of the nanoprobes, resulting in a linear increase in the signal of 4-MBA at 1585 cm^{-1} with concentration. This sensor attained an exceptionally low detection limit of 3×10^{-10} M and demonstrated favorable biocompatibility.

Table 5. Analytical efficacy of SERS tests for the identification of cadmium (Cd^{2+}) and chromium (Cr^{3+}) ions.

Nanostructure	Ligand	Linear Range	LOD	Method	Evaluation	Ion	Ref.
AuNPs	Alizarin / MPA / PDCA	—	89 pM (10 ppt)	Molecular Probe Engineering	Ultrasensitive	Cd^{2+}	[102]
AuNPs	Dopamine (DA)	10^{-4}–10^{-8} M	10 nM	Molecular Probe Engineering	Wide linear range	Cd^{2+}	[103]
AuNPs	R6G / GSH	4.45–178 μM (0.5–20 ppm)	89 nM (10 ppb)	Special Response Mechanisms	—	Cd^{2+}	[104]
AuNPs	Tween 20 / Citrate	50–200 nM	50 nM	Molecular Probe Engineering	—	Cr^{3+}	[105]
AgNPs	EDTA	—	0.5 μM	Molecular Probe Engineering	—	Cr^{3+}	[106]
Au-core/Ag-shell	4-MBA / DL-MSA	—	0.3 nM	Plasmonic nanohybrid design	Ultrasensitive	Cr^{3+}	[107]

4.2. Transition Metal and Other Metal Ions

Copper ions (Cu^{2+}), being redox-active metals, can function as coordination centers to promote aggregation or modify probe surface characteristics via catalytic activity. Li et al. [108] utilized L-cysteine-modified silver nanoparticles at an early stage. Utilizing the mechanism in which Cu^{2+} or Hg^{2+} forms insoluble inner complexes with surface ligands to promote aggregation, they successfully mitigated ionic interference by including SCN^- as a masking agent, resulting in high-sensitivity SERS detection of Cu^{2+} (LOD 10 pM) and Hg^{2+} (LOD 1 pM). Unlike the previously stated methodologies employing exogenous probes, Ly et al. [109] introduced an innovative mechanism centered on the redox dissociation of glycine (GLY). Cu^{2+} was found to significantly stimulate the aggregation of AuNPs and facilitate the conversion of GLY into cyano (CN) species on positively charged surfaces, resulting in a pronounced distinctive peak in the Raman silent area (~2108 cm^{-1}). This technique exhibited a detection limit (LOD) of 500 nM and a linear range of 0 to 10 μM in the study of real river water and HeLa cell imaging. Xu et al. [110] investigated the dual role of polyvinylpyrrolidone (PVP) as a stabilizer and a recognition element in an AgNPs system. They verified that Cu^{2+} functions as a cross-linker to facilitate aggregation and developed a ratiometric detection method utilizing the intensity ratio of PVP's intrinsic Raman peaks (I_{845}/I_{899}), attaining a linear range of 0.01–2 μM and a detection limit of 3 nM. To tackle the intricate background interference in biological matrices, Wang et al. [111] developed a probe co-modified with L-cysteine and 4-mercaptobenzonitrile. In a similar manner, they employed copper ion-induced aggregation to activate the signal in the Raman quiet

 doi:10.20944/preprints202601.1310.v1

region (2220 cm^{-1}), thereby accomplishing interference-free intracellular detection (LOD 0.055 μM, linear range 1 μM to 10 mM).

Feng et al. [112] developed a smart probe utilizing PNIPAM-functionalized gold nanogap particles (AuNNPs) for clinical in vitro diagnostics. This technique employed a Cu^{2+} coordination-induced particle aggregation mechanism to attain accurate SERS measurement of Cu^{2+} (LOD 57.4 μM, linear range 0–18 mM) by analyzing the signal ratio of the surface reporter molecule (MBN) to the internal standard molecule (NAT) (I_{2223}/I_{1378}). The ratiometric technique illustrated in Figure 11 exhibited significant practical use in the screening of Wilson's disease (WD). The probe successfully mitigated urine matrix interference by leveraging the self-calibration effect of the internal standard. Detection results indicated that Cu^{2+} concentrations in urine samples from Wilson's disease patients (~11.68 mM) were markedly elevated compared to those in the healthy control group (~0.454 mM) and the clinical diagnostic threshold (1.56 mM), hence affirming the efficacy of this approach for early illness identification.

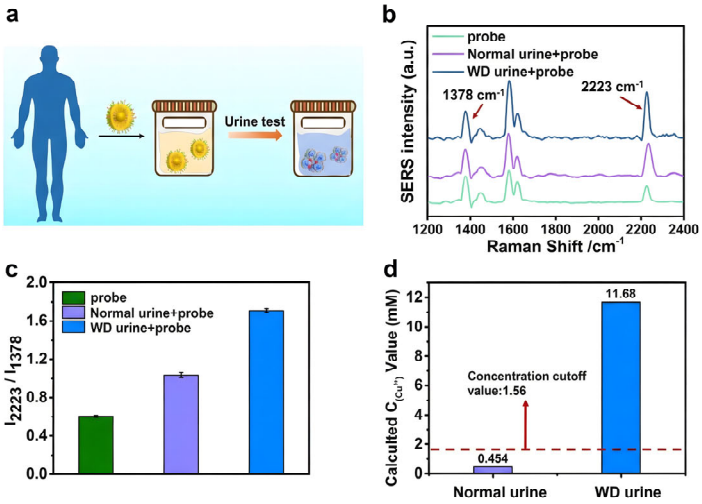

Figure 11. Practical implementation of the ratiometric SERS probe for the diagnosis of Wilson's disease (WD).

To tackle the problem of intricate matrix interference in real water bodies, Hsieh and Huang [113] developed magnetic functional materials to create Fe_3O_4@SiO_2-Ag-4MBA core-shell nanoprobes. This technique integrated the twin benefits of physical magnetic aggregation and chemically induced aggregation: an external magnetic field initially concentrated and separated the probes, subsequently followed by the close aggregation of particles facilitated by the bidentate coordination between Cu^{2+} and MBA. This design not only successfully mitigated matrix effects through magnetic separation but also markedly improved sensitivity through dual aggregation (LOD 0.421 ppm, linear range 0.5–20 ppm). It demonstrated enhanced anti-interference properties, especially against Fe^{2+} and Zn^{2+}, offering an effective solution for the swift on-site analysis of intricate environmental samples. Guo et al. [114] devised a novel "core-satellite" assembly strategy. They employed 4-mercaptobenzoic acid (MBA)-modified AgNPs as the "core" and 4-mercaptopyridine (Mpy)-modified AuNPs as "satellites". Cu^{2+} functioned as a metal linker, specifically connecting the carboxyl groups and pyridine nitrogen atoms, so facilitating the formation of Ag-Au heterostructures. This method accomplished visual colorimetric detection (LOD 0.032 μM) and, crucially, the high-density hotspots generated in the core-satellite gaps diminished the SERS detection limit to 0.6 pM, exhibiting a robust linear response from 1 pM to 100 μM, significantly below the EPA drinking water standard.

Integrated colorimetric and SERS dual-mode sensing technologies leverage the corroboration of macroscopic color alterations and microscopic spectral signatures to attain extremely reliable detection of copper ions (Cu^{2+}). Kumar et al. [115] introduced a high-performance dual-mode sensing

 doi:10.20944/preprints202601.1310.v1

approach utilizing Cystine-Tryptophan (CW) dipeptide-modified gold nanoparticles. The CW dipeptide in this system had distinctive "dual-function" properties: it acted as a particular capture probe for Cu^{2+} while employing its indole ring as an intrinsic Raman reporter. Cu^{2+} facilitated multidentate coordination with sulfur, indole nitrogen, and carbonyl oxygen within the peptide chain, resulting in the regulated aggregation of AuNPs and the formation of high-density electromagnetic hotspots (Figure 12A). The aggregation action not only altered the solution's color from red to blue (colorimetric LOD 76 nM) but also produced a substantial linear amplification of the SERS signal at 1416 cm^{-1} (Figure 12B-C). This work additionally integrated dry-state Raman mapping technique. Through visual examination of the signal distribution on the surface of dried droplets (Figure 12E-F), the probe's signal homogeneity at low concentrations was effectively confirmed, finally facilitating ultrasensitive detection down to 10 pM. Moreover, portable test strips designed utilizing this technique exhibited remarkable environmental stability, affirming the practical applicability of this strategy for point-of-care testing (POCT). Zheng et al. [116] developed a tri-modal sensing platform utilizing Schiff base ligand (BAMH)-modified gold nanorods (GNRs) to augment detection dimensionality. This approach employed the robust chelation between Cu^{2+} and BAMH ($K_a = 1.32 \times 10^7\ M^{-1}$) to facilitate the self-assembly of GNRs. This action concurrently initiated three signal alterations: a redshift of the LSPR peak (colorimetric), fluorescence quenching (fluorescence mode), and a notable amplification of the SERS signal at 1940 cm^{-1}. The reciprocal validation of these three modalities significantly diminished the likelihood of false positives, and this approach has been effectively utilized for detection in other domains, including ambient water samples and biological fluids (saliva, urine).

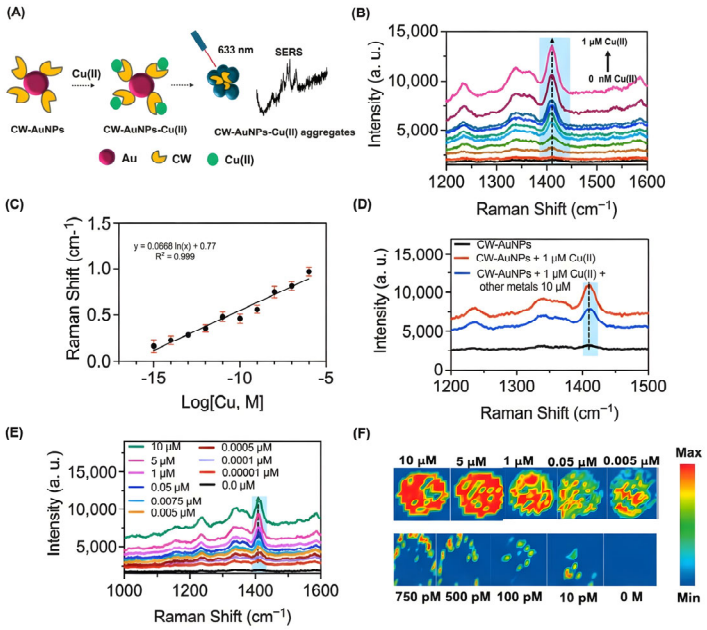

Figure 12. Schematic representation of the SERS sensing process utilizing Cu2+-induced aggregation of peptide-functionalized AuNPs and its analytical efficacy [115].

The catalytic activity or redox characteristics of Cu^{2+} facilitate the development of response systems predicated on "chemical shearing" or "redispersion" mechanisms. Li et al. [117] introduced a "label-free" biomacromolecule shearing technique via a Fenton-like reaction. This approach utilizes Cu^{2+} to catalyze ascorbic acid, producing highly oxidative hydroxyl radicals (•OH) that oxidatively split the protective layer of biomacromolecules (such as HSA, BSA, or DNA) surrounding the AuNPs, in contrast to standard coordination cross-linking. The deprotected AuNPs aggregate in a saline solution, activating the SERS signal. This "Signal-on" mechanism prevents the synthesis of intricate

 doi:10.20944/preprints202601.1310.v1

ligands. The results demonstrated that SERS had a robust linear response within the range of 0.025 to 25 μmol/L, with a detection limit of 0.008 μmol/L.

Utilizing the strong attraction of Fe^{3+} for oxygen atoms, natural extracts abundant in oxygen-containing functional groups can facilitate precise detection. Guo et al. [118] employed the exceptional affinity of iron ions for oxygen atoms to develop a silver nanoparticle (AgNPs) system functionalized with phytic acid (IP6) and modified with Rhodamine 6G (R6G). IP6, abundant in phosphate groups, establishes persistent Fe-O chelation complexes with Fe^{3+}, resulting in the reduction of interparticle distances to around 2.36 nm, thereby creating high-density SERS "hotspots". This approach, utilizing R6G as the signal reporter, attained a LOD of 0.28 ppm and a linear range of 11.2–39.2 ppm. Moreover, the negatively charged IP6 layer efficiently protected against interference from ambient ions.Xu et al. [119] developed a very sensitive label-free analytical method for Fe^{2+} detection by leveraging the synergistic effects of coordination chemistry and surface-enhanced resonance Raman scattering (SERRS). They chose 2,2'-bipyridine (Bpy) as the probe chemical. The introduction of Fe^{2+} prompts a conformational shift of Bpy from trans to cis, hence resulting in the creation of a stable $[Fe(Bpy)_3]^{2+}$ complex. This compound efficiently promotes AgNP aggregation to create electromagnetic hotspots and features an absorption peak at 522 nm, which closely aligns with the excitation light source at 532 nm, resulting in robust resonance Raman enhancement signals. Utilizing this dual enhancement process, the approach attained a broad linear range of 10^{-11} to 10^{-7} M and an exceptionally low detection limit of 5.73 pM. Moreover, leveraging the particular coordination configuration, the probe demonstrated exceptional anti-interference capability; as illustrated in Figure 13, the sensor preserved a distinct spectral response to Fe^{2+} even in the presence of various competing metal ions, affirming its applicability in complex environments.

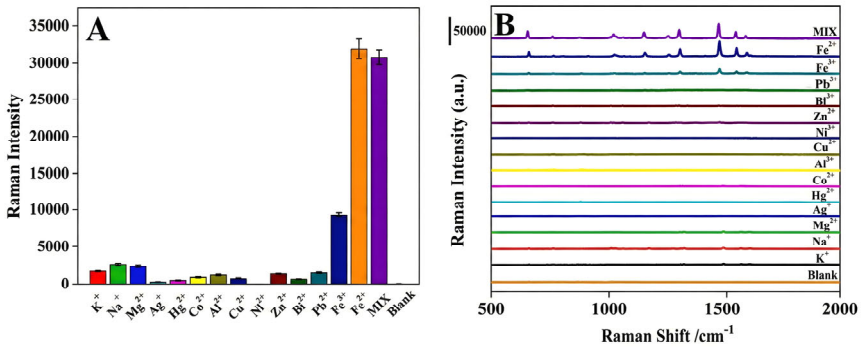

Figure 13. Assessment of selectivity for the Bpy-based SERRS test in detecting Fe^{2+}. Comparison of SERS intensities at 1487 cm^{-1} in the presence of Fe^{2+} and other interfering metal ions. (B) Corresponding SERS spectra illustrating the distinct signal response elicited by the creation of the $[Fe(Bpy)_3]^{2+}$ complex [119].

Table 6. Analytical efficacy of SERS tests for the identification of copper (Cu^{2+}) and iron (Fe) ions.

Nanostructure	Ligand	Linear Range	LOD	Method	Evaluation	Ion	Ref.
AuNPs	Glycine (GLY)	0–10 μM	500 nM	Special Response Mechanisms	—	Cu^{2+}	[109]
AgNPs	PVP	0.01–2 μM	3 nM	Molecular Probe Engineering	Self-calibrated	Cu^{2+}	[110]
AgNPs	L-Cys & 4-MBN	1 μM–10 mM	0.055 μM	Molecular Probe Engineering	—	Cu^{2+}	[111]

 doi:10.20944/preprints202601.1310.v1

AuNNPs	PNIPAM / MBN	0–18 mM	57.4 μM	Molecular Probe Engineering	Self-calibrated	Cu^{2+}	[112]
Fe_3O_4@SiO_2-Ag	4-MBA	7.9–315 μM (0.5–20 ppm)	6.6 μM (0.421 ppm)	Plasmonic nanohybrid design	—	Cu^{2+}	[113]
Ag-Au (Core-Satellite)	MBA & Mpy	1 pM–100 μM	0.6 pM	Plasmonic nanohybrid design	Ultrasensitive & Wide linear range	Cu^{2+}	[114]
AuNPs	Peptide (CW)	—	10 pM	Multimodal sensing & Molecular Probe Engineering	Sensitive & Portable	Cu^{2+}	[115]
AuNPs	Ascorbic acid / BSA	0.025–25 μM	8 nM	Special Response Mechanisms	—	Cu^{2+}	[117]
AgNPs	Phytic acid (IP6)	200–700 μM (11.2–39.2 ppm)	5 μM (0.28 ppm)	Green Synthesis Strategies	—	Fe^{3+}	[118]
AgNPs	2,2'-bipyridine (Bpy)	10^{-11}–10^{-7} M	5.73 pM	Molecular Probe Engineering		Fe^{2+}	[119]

Li et al. [120] were pioneers in developing AgNP probes co-modified with GSH and 4-mercaptopyridine (4-MPY) for the detection of the very hazardous metalloid arsenic (As^{3+}). By exploiting the unique affinity of As^{3+} for the oxygen-rich moieties in GSH (As-O linkages) to promote the aggregation of silver nanoparticles, they amplified the SERS signal of the surface beacon 4-MPY, attaining high-sensitivity detection of trace As^{3+} in water (LOD 0.76 ppb) across a linear range of 4–300 ppb. Specific detection of induced aggregation for Ba^{2+} can be accomplished via sulfur-containing carboxylic acid ligands. Charkova [121] synthesized 4-mercaptophenylacetic acid (MPAA) functionalized AgNPs probes for the detection of biologically harmful barium ions (Ba^{2+}). Ba^{2+} establishes unique "molecular bridges" with the terminal carboxyl groups of MPAA, resulting in the aggregation of nanoparticles into large clusters (>0.5 μm). SERS technology effectively detected subtle fluctuations in benzene ring breathing vibrations during aggregation, attaining an exceptionally low detection limit of 10^{-15} M (femtomolar level). This indicates a sensitivity enhancement of six orders of magnitude relative to conventional nanocolorimetric techniques, validating the practical utility of this approach in environmental toxicity assessment. The precise identification of rare earth elements (REEs) has always posed difficulties owing to their closely related chemical characteristics. Jin et al. [122] employed citrate-capped AgNPs to develop a SERS classification platform for La^{3+} and Gd^{3+}. This study examined the influence of variations in ionic 4f electron configurations (La^{3+} as $4f^0$ and Gd^{3+} as $4f^7$) on Raman scattering cross-sections. Experiments and DFT simulations revealed that the coordination of RE^{3+} with citrate molecules not only facilitated AgNP aggregation but also resulted in a notable ion dependence of the peak intensity ratio at 1065 cm^{-1} and 1315 cm^{-1} (I_{1065}/I_{1315}). The spectrum feature differences dependent on spin states, as illustrated in Figure 14, effectively facilitated the qualitative differentiation of these two rare earth ions.

 doi:10.20944/preprints202601.1310.v1

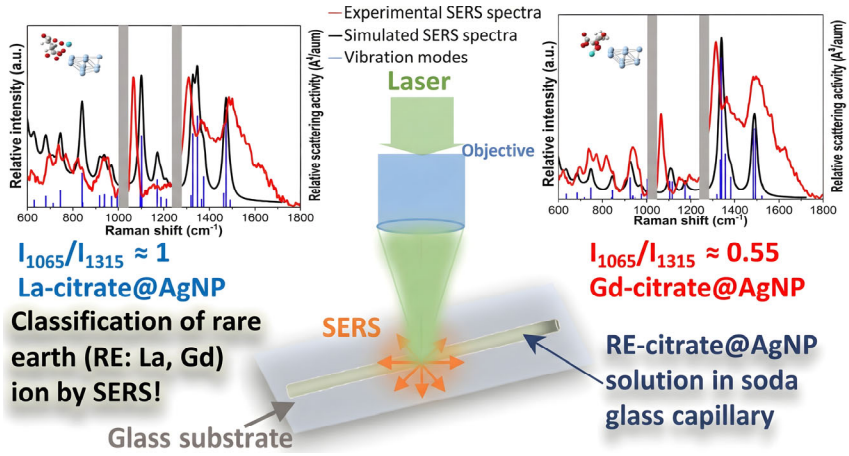

Figure 14. SERS differentiation of La^{3+} and Gd^{3+} with citrate-capped AgNPs. The spectra display unique intensity ratios (I_{1065}/I_{1315}) resulting from spin-state variations ($4f^0$ vs. $4f^7$), validated by DFT computations [122].

4.3. Multi-Metal Ions

This section examines multifunctional SERS sensing systems that can concurrently detect or differentiate several metal ions. In real environmental monitoring, the coexistence of numerous pollutants necessitates the development of sensors with broad-spectrum responses or multi-channel recognition capabilities, which is of considerable importance.

Employing biomass molecules abundant in functional groups as reducing and capping agents facilitates the eco-friendly synthesis of nanomaterials and enhances sensors' broad-spectrum responsiveness to various metal ions. Sharma and associates [123–125] have performed a series of comprehensive investigations in this domain, including microwave-assisted techniques to swiftly synthesis diverse functionalized AgNPs. Sharma et al. employed the carboxyl and hydroxyl groups on pectin chains in a pectin-based system to facilitate the aggregation of AgNPs in the presence of ions like Cr^{3+}, Se^{4+}, and Mn^{2+}. This device accomplished dual-mode SERS and colorimetric detection by observing alterations in distinctive Raman peaks (e.g., Se^{4+} at 432 cm^{-1}, Mn^{2+} at 586 cm^{-1}), with a LOD for Cr^{6+} as low as 6.40 μM. Subsequently, the team broadened their research to a lignin-functionalized system, demonstrating that lignin-capped AgNPs displayed remarkable colorimetric responses to Co^{2+}, Cr^{3+}, and Mn^{2+}, and accomplished high-sensitivity fingerprint identification of Mn^{2+} in SERS mode through signal amplification at 595 cm^{-1} (LOD 0.06 mM). In their investigation of ferulic acid, they further clarified the mechanisms differentiating the colorimetric alterations generated by Fe^{2+} from the SERS signal amplification induced by Cr^{3+} at 240 cm^{-1}. This body of work illustrates that the many oxygen sites in biomass molecules can function as universal trapping agents for various metal ions, presenting considerable promise for on-site screening when integrated with portable instruments.

In contrast to the intricate configurations of biomass molecules, the modification with structurally specified small-molecule Raman beacons enables the development of more accurate quantitative models. Daublytė et al. [126] developed a conventional system of 4-MBA modified AgNPs for the detection of divalent metal ions (Cu^{2+}, Fe^{2+}, Co^{2+}, Pb^{2+}, etc.). The fundamental mechanism entails the creation of $(-COO^-)_2Me^{2+}$ "bridging complexes" between metal ions and surface carboxyl groups. This particular chemical bridging causes substantial aggregation of AgNPs, resulting in notable SERS amplification at 1585 cm^{-1}. The probe had the greatest affinity for Cu^{2+} (LOD 2.5×10^{-7} M) while also exhibiting a broad response to other divalent ions, hence validating the utility of carboxyl coordination-based aggregation techniques for the assessment of total divalent heavy metals. Kappen et al. [127] employed graphene quantum dots (GQDs) to modify AgNPs and conducted a comprehensive analysis of the distinct methods through which various metal ions induce alterations in SERS signals. The research revealed that the mechanisms of action differ significantly among ions: Cd^{2+} interacts with functional groups on the GQD surface, causing AgNPs

 doi:10.20944/preprints202601.1310.v1

to aggregate in chain-like formations; Pb^{2+} induces an etching effect on AgNPs and facilitates the formation of PbO; whereas Hg^{2+} instigates a redox reaction, resulting in the dissolution of Ag^0 and the reduction/deposition of Hg^0. This study on Ag-GQD composites surpasses basic "aggregation-enhancement" models; by linking morphological changes (e.g., sphere-to-chain transition, etching) with spectral responses, it offers a comprehensive physicochemical framework for differentiating various heavy metal ions.

5. Conclusions

The accurate monitoring and dynamic analysis of metal ions are crucial for ensuring ecological safety and protecting human health. Due to the constraints of conventional bulky instrumental analysis methods in swift on-site detection applications, the advancement of detection approaches that integrate high sensitivity, affordability, and convenience has emerged as a focal point of research in analytical chemistry. Colorimetric analysis and SERS techniques utilizing the aggregation effect of Au/Ag NPs, due to their distinctive LSPR characteristics and electromagnetic field amplification mechanisms, offer effective methods for the qualitative identification and quantitative extraction of metal ions. This review comprehensively outlines methodological advancements in this domain, focusing on green synthesis techniques utilizing biomass extracts, Ligand engineering for targeted surface recognition, and sensing mechanisms that encompass oxidative etching, coordination bridging, and biomolecular conformational transitions. Moreover, the incorporation of physically assisted preparation methods, solid-phase support devices, and intelligent readout systems integrated with machine learning algorithms has significantly broadened the application potential of colorimetric and SERS techniques reliant on Au/Ag NPs aggregation in intricate environments.

Significant advancements have been achieved in enhancing detection efficacy. Notable research has accomplished "ultrasensitive" detection of trace metal ions, with LODs for certain technologies exceeding the criteria set by the World Health Organization (WHO) and pertinent environmental guidelines. Simultaneously, smart terminal-based detection devices reconcile "high sensitivity" with "on-site portability," confirming the viability of point-of-care testing (POCT) in resource-constrained areas. The implementation of ratiometric measurements and dual-mode signal complementary techniques has provided sensors with "self-calibration" skills, significantly enhancing the reliability of analyses in complicated matrices. Nonetheless, detection approaches reliant on aggregation effects continue to encounter several challenges: The colloidal stability of nanoparticles is readily disrupted by non-specific variables, including ambient ionic strength, pH, and temperature, resulting in false-positive findings. The randomness of the aggregation process leads to an inhomogeneous distribution of SERS "hotspots," hence impacting signal repeatability and quantitative precision. Ultimately, in genuine complicated samples, the competing coordination of various coexisting ions may diminish probe selectivity, and certain probes reliant on irreversible chemical reactions encounter difficulties in maintaining continual online monitoring.

Recent research advancements suggest that metal ion detection utilizing Au/Ag nanoclusters is progressively evolving towards a multidisciplinary integration. Future investigations are expected to focus on the following directions: 1) Formulating surface modification techniques with enhanced anti-interference properties and environmental adaptation to augment the long-term stability and specificity of probes in intricate matrices such as whole blood and wastewater; 2) Enhancing the utilization of chemometrics and artificial intelligence algorithms in spectral data processing to resolve non-linear signal responses and multiple interference challenges; 3) Advancing the downsizing and integration of sensing platforms by amalgamating microfluidics with wearable devices to facilitate high-throughput and in situ dynamic monitoring of metal ions; and 4) Investigating nontraditional physical mechanisms, such as interfacial electron spin phenomena, to overcome obstacles in differentiating chemically analogous ions or congeners.

In conclusion, colorimetric and SERS sensing systems utilizing the Au/Ag aggregation effect exhibit extensive potential in metal ion detection. Despite the pressing need to resolve technical impediments related to stability and reproducibility, the standardization of nanomaterial synthesis,

 doi:10.20944/preprints202601.1310.v1

an enhanced comprehension of surface ligand chemistry, and the advancement of data analysis techniques position this technology to assume a more pivotal role in environmental monitoring, food safety, and biomedical diagnostics, facilitating a successful transition from laboratory research to practical field applications.

Author Contributions: L.Y. and S.W. conceived the idea and designed the framework of the review. S.W. was responsible for the literature collection, summarization, and the writing of the original draft. Y.F. and J.H. assisted with the literature research and data organization. L.Y. provided overall guidance and critically revised the manuscript. C.Z., Y.M. and G.H. participated in the supervision and the review of the paper. All authors have read and agreed to the published version of the manuscript.

Funding: This work was supported by the Zhejiang Provincial Natural Science Foundation (No. LQN25F050002)

Institutional Review Board Statement: Not applicable.

Informed Consent Statement: Not applicable.
Data Availability Statement: Data are available upon request to the corresponding author.

Conflicts of Interest: The authors declare no conflicts of interest.

References

1. Hasan, Z.; Jamal, A.; Hassan, T. Different Approaches for Detecting Heavy Metal Ions. In *Remediation of Heavy Metals: Sustainable Technologies and Recent Advances*; Selvasembian, R., Thokchom, B., Singh, P., Jawad, A.H., Gwenzi, W., Eds.; John Wiley & Sons: Hoboken, NJ, USA, 2023; pp. 83–107. https://doi.org/https://doi.org/10.1002/9781119853589.ch5.
2. Ali, H.; Khan, E.; Ilahi, I. Environmental Chemistry and Ecotoxicology of Hazardous Heavy Metals: Environmental Persistence, Toxicity, and Bioaccumulation. *J. Chem.* **2019**, *2019*, 1–14. https://doi.org/10.1155/2019/6730305
3. Rajkumar, N.; Chitturi, C. M. K.; Lavanya, K.; Subhashini, V.; Shamshad, S.; Seethamma, G. Consequences of Toxic Heavy Metals on Environment and Human Health: A Review. *Uttar Pradesh J. Zool.* **2025**, *46*, 198–207. https://doi.org/10.56557/upjoz/2025/v46i94936.
4. Quintanar, L.; Lim, M. H. Metal Ions and Degenerative Diseases. *J. Biol. Inorg. Chem.* **2019**, *24*, 1137–1139. https://doi.org/10.1007/s00775-019-01744-4.
5. Zhao, Z. Iron and Oxidizing Species in Oxidative Stress and Alzheimer's Disease. *Aging Med.* **2019**, *2*, 82–87. https://doi.org/10.1002/agm2.12074.
6. Kronzucker, H. J.; Coskun, D.; Schulze, L. M.; Wong, J. R.; Britto, D. T. Sodium as Nutrient and Toxicant. *Plant Soil* **2013**, *369*, 1–23. https://doi.org/10.1007/s11104-013-1801-2.
7. Alasfar, R. H.; Isaifan, R. J. Aluminum Environmental Pollution: The Silent Killer. *Environ. Sci. Pollut. Res.* **2021**, *28*, 44587–44597. https://doi.org/10.1007/s11356-021-14700-0.
8. Itoh, A.; Yaida, A.; Zhu, Y. Potential Anthropogenic Pollution of High-Technology Metals with a Focus on Rare Earth Elements in Environmental Water. *Anal. Sci.* **2020**, *37*, 131–143. https://doi.org/10.2116/analsci.20SAR16.
9. Clases, D.; Gonzalez de Vega, R. Facets of ICP-MS and Their Potential in the Medical Sciences—Part 1: Fundamentals, Stand-Alone and Hyphenated Techniques. *Anal. Bioanal. Chem.* **2022**, *414*, 7337–7361. https://doi.org/10.1007/s00216-022-04259-1.
10. Barik, P.; Mehta, A.; Makhija, R.; Saha, M.; Asati, V. Recent Advancements in Inductively Coupled Plasma Mass Spectrometry in Trace Element Analysis. *Curr. Anal. Chem.* **2025**, *21*, 1129–1148. https://doi.org/10.2174/0115734110333019241114050058.
11. Khan, S. R.; Sharma, B.; Chawla, P. A.; Bhatia, R. Inductively Coupled Plasma Optical Emission Spectrometry (ICP-OES): A Powerful Analytical Technique for Elemental Analysis. *Food Anal. Methods* **2021**, *15*, 666–688. https://doi.org/10.1007/s12161-021-02148-4.
12. Ogunfowokan, A. O.; Adekunle, A. S.; Oyebode, B. A.; Oyekunle, J. A. O.; Komolafe, A. O.; Omoniyi-Esan, G. O. Determination of Heavy Metals in Urine of Patients and Tissue of Corpses by Atomic Absorption

 doi:10.20944/preprints202601.1310.v1

Spectroscopy. *Chem. Afr. J. Tunisian Chem. Soc.* **2019**, *2*, 699–712. https://doi.org/10.1007/s42250-019-00073-y.

13. Hu, T.; Lai, Q.; Fan, W.; Zhang, Y.; Liu, Z. Advances in Portable Heavy Metal Ion Sensors. *Sensors* **2023**, *23*, 4125. https://doi.org/10.3390/s23084125.
14. Ataş, H. B.; Kenar, A.; Taştekin, M. An Electronic Tongue for Simultaneous Determination of Ca2+, Mg2+, K+ and NH4+ in Water Samples by Multivariate Calibration Methods. *Talanta* **2020**, *217*, 121110. https://doi.org/10.1016/j.talanta.2020.121110.
15. Li, L.; Wang, J.; Xu, S.; Li, C.; Dong, B. Recent Progress in Fluorescent Probes For Metal Ion Detection. *Front. Chem.* **2022**, *10*, 875241. https://doi.org/10.3389/fchem.2022.875241.
16. Noreldeen, H. A. A.; Zhu, C.-T.; Huang, K.-Y.; Peng, H.-P.; Deng, H.-H.; Chen, W. A Double Probe-Based Fluorescence Sensor Array to Detect Rare Earth Element Ions. *Analyst* **2025**, *150*, 612–619. https://doi.org/10.1039/d4an01520g.
17. Xu, G.; Song, P.; Xia, L. Examples in the Detection of Heavy Metal Ions Based on Surface-Enhanced Raman Scattering Spectroscopy. *Nanophotonics* **2021**, *10*, 4419–4445. https://doi.org/10.1515/nanoph-2021-0363.
18. Shellaiah, M.; Sun, K.-W. Review on Anti-Aggregation-Enabled Colorimetric Sensing Applications of Gold and Silver Nanoparticles. *Chemosensors* **2022**, *10*, 536. https://doi.org/10.3390/chemosensors10120536.
19. Lee, J.-S. Silver Nanomaterials for the Detection of Chemical and Biological Targets. *Nanotechnol. Rev.* **2014**, *3*, 499–513. https://doi.org/10.1515/ntrev-2014-0017.
20. Rajkumar, G.; Sundar, R. Sonochemical-Assisted Eco-Friendly Synthesis of Silver Nanoparticles (AgNPs) Using Avocado Seed Extract: Naked-Eye Selective Colorimetric Recognition of Hg2+ Ions in Aqueous Medium. *J. Mol. Liq.* **2022**, *368*, 120638. https://doi.org/10.1016/j.molliq.2022.120638.
21. Patra, S.; Golder, A. K.; Uppaluri, R. V. S. Mature Green Tea Leaves Derived CDs as Both Reducing Agent and Stabilizer for Synthesis of CD-AgNPs Composite for Hg(II) Ions Detection. *Next Nanotechnol.* **2025**, *8*, 100219. https://doi.org/10.1016/j.nxnano.2025.100219.
22. Issarangkura Na Ayutthaya, P.; Vongboot, M. Two Principles for Colorimetric Detections of Cr6+ Using Polyurethane Foam—Gold Nanoparticles Composite. *Univers. J. Green Chem.* **2024**, *2*, 172–186. https://doi.org/10.37256/ujgc.2220244938.
23. Gholami, M. D.; Alzubaidi, F. M.; Liu, Q.; Izake, E. L.; Sonar, P. Rapidly and Simply Detecting Cr (VI) in Aqueous Media via a Diketopyrrolopyrrole-Based Chemosensor with Both High Selectivity and Low LOD. *Anal. Chim. Acta* **2024**, *1316*, 342861. https://doi.org/10.1016/j.aca.2024.342861.
24. Singh, H.; Bamrah, A.; Bhardwaj, S. K.; Deep, A.; Khatri, M.; Brown, R. J. C.; Bhardwaj, N.; Kim, K.-H. Recent Advances in the Application of Noble Metal Nanoparticles in Colorimetric Sensors for Lead Ions. *Environ. Sci.-Nano* **2021**, *8*, 863–889. https://doi.org/10.1039/d0en00963f.
25. Kant, T.; Shrivas, K.; Tejwani, A.; Tandey, K.; Sharma, A.; Gupta, S. Progress in the Design of Portable Colorimetric Chemical Sensing Devices. *Nanoscale* **2023**, *15*, 19016–19038. https://doi.org/10.1039/d3nr03803c.
26. Ouyang, H.; Ling, S.; Liang, A.; Jiang, Z. A Facile Aptamer-Regulating Gold Nanoplasmonic SERS Detection Strategy for Trace Lead Ions. *Sens. Actuator B-Chem.* **2018**, *258*, 739–744. https://doi.org/10.1016/j.snb.2017.12.009.
27. Docherty, J.; Mabbott, S.; Smith, W. E.; Reglinski, J.; Faulds, K.; Davidson, C.; Graham, D. Determination of Metal Ion Concentrations by SERS Using 2,2′-Bipyridyl Complexes. *Analyst* **2015**, *140*, 6538–6543. https://doi.org/10.1039/C5AN01525A.
28. Liu, C.; Wang, H.; Xu, S.; Li, H.; Lu, Y.; Zhu, C. Recyclable Multifunctional Magnetic Fe3O4@SiO2@Au Core/Shell Nanoparticles for SERS Detection of Hg (II). *Chemosensors* **2023**, *11*, 347. https://doi.org/10.3390/chemosensors11060347.
29. Li, Y.; Zhou, N.; Yan, J.; Cui, K.; Chu, Q.; Chen, X.; Luo, X.; Deng, X. A Dual-Signaling Surface-Enhanced Raman Spectroscopy Ratiometric Strategy for Ultrasensitive Hg2+ Detection Based on Au@Ag/COF Composites. *Food Chem.* **2024**, *456*, 139998. https://doi.org/10.1016/j.foodchem.2024.139998.
30. Zhao, Y.; Yamaguchi, Y.; Ni, Y.; Li, M.; Dou, X. A SERS-Based Capillary Sensor for the Detection of Mercury Ions in Environmental Water. *Spectroc. Acta Pt. A-Molec. Biomolec. Spectr.* **2020**, *233*, 118193. https://doi.org/10.1016/j.saa.2020.118193.

 doi:10.20944/preprints202601.1310.v1

31. Kang, Y.; Zhang, H.; Zhang, L.; Wu, T.; Sun, L.; Jiang, D.; Du, Y. In Situ Preparation of Ag Nanoparticles by Laser Photoreduction as SERS Substrate for Determination of Hg2+. *J. Raman Spectrosc.* **2016**, *48*, 399–404. https://doi.org/10.1002/jrs.5044.
32. Amirjani, A.; Haghshenas, D. F. Ag Nanostructures as the Surface Plasmon Resonance (SPR)-based Sensors: A Mechanistic Study with an Emphasis on Heavy Metallic Ions Detection. *Sens. Actuators B Chem.* **2018**, *273*, 1768–1779. https://doi.org/10.1016/j.snb.2018.07.089.
33. Suriati, G.; Mariatti, M.; Azizan, A. Synthesis of Silver Nanoparticles by Chemical Reduction Method: Effect of Reducing Agent and Surfactant Concentration. *Int. J. Automot. Mech. Eng.* **2022**, *10*, 1920–1927. https://doi.org/10.15282/ijame.10.2014.9.0160.
34. Do Thi, H.; Nghien Thi Ha, L.; Chu Viet, H. Seeded Growth Synthesis of Uniform Gold Nanoparticles with Controlled Diameters up to 220 Nm. *J. Electron. Mater.* **2021**, *50*, 5514–5521. https://doi.org/10.1007/s11664-021-09081-6.
35. Amirjani, A.; Haghshenas, D. F. Ag Nanostructures as the Surface Plasmon Resonance (SPR)-based Sensors: A Mechanistic Study with an Emphasis on Heavy Metallic Ions Detection. *Sens. Actuators B Chem.* **2018**, *273*, 1768–1779. https://doi.org/10.1016/j.snb.2018.07.089.
36. Pomal, N. C.; Bhatt, K. D.; Modi, K. M.; Desai, A. L.; Patel, N. P.; Kongor, A.; Kolivoška, V. Functionalized Silver Nanoparticles as Colorimetric and Fluorimetric Sensor for Environmentally Toxic Mercury Ions: An Overview. *J. Fluoresc.* **2021**, *31*, 635–649. https://doi.org/10.1007/s10895-021-02699-z.
37. Alvarez-Puebla, R. A.; Liz-Marzán, L. M. SERS Detection of Small Inorganic Molecules and Ions. *Angew. Chem.-Int. Edit.* **2012**, *51*, 11214–11223. https://doi.org/10.1002/anie.201204438.
38. Parakh, A.; Awate, A.; Barman, S. M.; Kadu, R. K.; Tulaskar, D. P.; Kulkarni, M. B.; Bhaiyya, M. Artificial Intelligence and Machine Learning for Colorimetric Detections: Techniques, Applications, and Future Prospects. *Trends Environ. Anal. Chem.* **2025**, *48*, e00280. https://doi.org/10.1016/j.teac.2025.e00280.
39. Town, R. M.; Buffle, J.; Duval, J. F. L.; van Leeuwen, H. P. Chemodynamics of Soft Charged Nanoparticles in Aquatic Media: Fundamental Concepts. *J. Phys. Chem. A* **2013**, *117*, 7643–7654. https://doi.org/10.1021/jp4044368.
40. Xu, B. Adsorption Behavior of Metal Cations on Gold Nanoparticle Surfaces Studied by Isothermal Titration Microcalorimetry. *J. Chin. Chem. Soc.* **2010**, *57*, 309–315. https://doi.org/10.1002/jccs.201000046.
41. Ngamchuea, K.; Batchelor-McAuley, C.; Sokolov, S. V.; Compton, R. G. Dynamics of Silver Nanoparticles in Aqueous Solution in the Presence of Metal Ions. *Anal. Chem.* **2017**, *89*, 10208–10215. https://doi.org/10.1021/acs.analchem.7b01470.
42. Toma, H. E.; Zamarion, V. M.; Toma, S. H.; Araki, K. The Coordination Chemistry at Gold Nanoparticles. *J. Braz. Chem. Soc.* **2010**, *21*, 1158–1176. https://doi.org/10.1590/S0103-50532010000700003.
43. Guan, H.; Harris, C.; Sun, S. Metal–Ligand Interactions and Their Roles in Controlling Nanoparticle Formation and Functions. *Acc. Chem. Res.* **2023**, *56*, 1591–1601. https://doi.org/10.1021/acs.accounts.3c00156.
44. Zheng, Y.; Zeng, J.; Ruditskiy, A.; Liu, M.; Xia, Y. Oxidative Etching and Its Role in Manipulating the Nucleation and Growth of Noble-Metal Nanocrystals. *Chem. Mater.* **2013**, *26*, 22–33. https://doi.org/10.1021/cm402023g.
45. Katanosaka, A.; Fostier, A.; Santos, E. Efeito do Hg2+ e dos Íons Cu2+, Fe2+, Ni2+, Sn2+ e Zn2+ na Estabilidade de Nanopartículas de Prata: Uma Prática Interdisciplinar de Nanotecnologia Experimental. *Quim. Nova* **2020**, *44*, 512–518. https://doi.org/10.21577/0100-4042.20170679.
46. Chopada, R.; Sarwate, R.; Kumar, V. Effect of Mild to Extreme pH, Temperature, and Ionic Strength on the Colloidal Stability of Differentially Capped Gold Nanoparticles. *J. Mol. Struct.* **2025**, *1323*, 140751. https://doi.org/10.1016/j.molstruc.2024.140751.
47. Zhang, Z.; Ye, X.; Liu, Q.; Liu, Y.; Liu, R. Colorimetric Detection of Cr3+ Based on Gold Nanoparticles Functionalized with 4-Mercaptobenzoic Acid. *J. Anal. Sci. Technol.* **2020**, *11*, 10. https://doi.org/10.1186/s40543-020-00209-7.
48. Memon, R.; Memon, A. A.; Balouch, A.; Shah, M. R.; Sherazi, S. T. H.; Memon, S. S.; Memon, K. Highly Selective Nanomolar Level Colorimetric Sensing of Cr3+ through Biosynthesized Gold Nanoparticles in the Presence of Cr6+. *Optik* **2021**, *248*, 168188. https://doi.org/10.1016/j.ijleo.2021.168188.

 doi:10.20944/preprints202601.1310.v1

49. Shellaiah, M.; Sun, K. W. Conjugation of Cysteamine Functionalized Nanodiamond to Gold Nanoparticles for pH Enhanced Colorimetric Detection of Cr3+ Ions Demonstrated by Real Water Sample Analysis. *Spectroc. Acta Pt. A-Molec. Biomolec. Spectr.* **2023**, *286*, 121962. https://doi.org/10.1016/j.saa.2022.121962.
50. Gunupuru, R.; Paul, P. Synthesis and Characterization of 2-Amino-5-Mercapto-1,3,4-Thiadiazole Functionalized Gold Nanoparticles and It's Use for Colorimetric Sensing of Cr3+ and Pb2+ in Aqueous Medium. *J. Indian Chem. Soc.* **2025**, *102*, 101566. https://doi.org/10.1016/j.jics.2025.101566.
51. Zhang, L.; Li, J.; Wang, J.; Yan, X.; Song, J.; Feng, F. An Ultra-Sensitive Colorimetric Sensing Platform for Simultaneous Detection of Moxifloxacin/Ciprofloxacin and Cr(III) Ions Based on Ammonium Thioglycolate Functionalized Gold Nanoparticles. *Sensors* **2025**, *25*, 3228. https://doi.org/10.3390/s25103228.
52. Shi, J.; Wu, S.; Xue, Y.; Xie, Q.; Danzeng, Q.; Liu, C.; Zhou, C.-H. Fluorescence/Colorimetric Dual-Signal Sensor Based on Carbon Dots and Gold Nanoparticles for Visual Quantification of Cr3+. *Microchim. Acta* **2024**, *191*, 571. https://doi.org/10.1007/s00604-024-06645-1.
53. Rajamanikandan, R.; Ilanchelian, M.; Ju, H. Smartphone-Enabled Colorimetric Visual Quantification of Highly Hazardous Trivalent Chromium Ions in Environmental Waters and Catalytic Reduction of p-Nitroaniline by Thiol-Functionalized Gold Nanoparticles. *Chemosphere* **2023**, *340*, 139838. https://doi.org/10.1016/j.chemosphere.2023.139838.
54. Moradifar, B.; Afkhami, A.; Madrakian, T.; Jalali Sarvestani, M. R.; Khalili, S. Rapid, Simple and Highly Selective Determination of Chromium(III) in Aqueous Samples by a Microfluidic Cell Coupled to a Smartphone-Based Colorimetric-Sensing Detector. *J. Iran. Chem. Soc.* **2025**, *22*, 605–613. https://doi.org/10.1007/s13738-025-03172-5.
55. Sharma, S.; Sharma, S. K.; Tiwari, A.; Jaiswal, A.; Uttam, K. N. Chlorophyll Coated Silver Nanoparticles Synthesized by Microwave Assisted Method for the Colorimetric Detection of Cr (VI) Ions in Aqueous Medium. *Anal. Lett.* **2023**, *57*, 940–952. https://doi.org/10.1080/00032719.2023.2233034.
56. Skiba, M.; Vorobyova, V. Sustainable PVP-Capped Gold Nanoparticles Synthesis "Green" Chemistry Plasma-Liquid Method and Colorimetric Activity for Water Pollutant Chromium Ion (Cr(VI)). *Gold Bull.* **2025**, *58*, 15. https://doi.org/10.1007/s13404-025-00368-8.
57. Muthwa, S. F.; Zulu, N. S.; Kistan, M.; Onwubu, S. C.; Shumbula, N. P.; Moloto, N.; Mpelane, S.; Hlatshwayo, T.; Mlambo, M.; Mdluli, P. S. Unravelling Mechanism for Detecting Chromium on Functionalized Gold Nanoparticles via a Smartphone and Spectrophotometric-Based Systems Supported by CIEL*ab** Colour Space and Molecular Dynamics. *J. Mol. Struct.* **2023**, *1274*, 134394. https://doi.org/10.1016/j.molstruc.2022.134394.
58. Karn-orachai, K.; Wattanasin, P.; Ngamaroonchote, A. Colorimetric Sensor for Cr(VI) Ion Detection in Tap Water Using a Combination of AuNPs and AgNPs. *ACS Omega* **2024**, *9*, 26472–26483. https://doi.org/10.1021/acsomega.4c02699.
59. Esquivel-Rincón, J. O.; Vilchis-Nestor, A. R.; Ruiz-Ruiz, V. F.; Olea-Mejía, O. F. Advancements in On-Site Heavy Metal Detection: Characterizing and Sensitive Hg2+ Sensing of Silver Spheroid Nanoparticles Obtained by Laser Ablation Synthesis in Solution. *Microchem. J.* **2024**, *206*, 111597. https://doi.org/10.1016/j.microc.2024.111597.
60. Tewari, S.; Sahani, S.; Yaduvanshi, N.; Painuli, R.; Sankararamakrishnan, N.; Dwivedi, J.; Sharma, S.; Han, S. S. Green Synthesized AgNPs as a Probe for Colorimetric Detection of Hg (II) Ions in Aqueous Medium and Fluorescent Imaging in Liver Cell Lines and Its Antibacterial Activity. *Discov. Nano* **2024**, *19*, 78. https://doi.org/10.1186/s11671-024-04014-8.
61. Thepwat, P.; Saenchoopa, A.; Onnet, W.; Namcharee, P.; Sanmanee, C.; Plaeyao, K.; Kulchat, S.; Kosolwattana, S. The Synthesis and Study of Carboxymethyl Cellulose from Water Hyacinth Biomass Stabilized Silver Nanoparticles for a Colorimetric Detection Sensor of Hg(II) Ions. *RSC Adv.* **2025**, *15*, 41241–41252. https://doi.org/10.1039/D5RA04757A.
62. Mume, L.; Kebede, M.; Bekana, D.; Tan, Z.; Amde, M. Salvia Tiliifolia Leaf Extract-Based Silver Nanoparticles for Colorimetric Detection of Hg(II) in Food and Environmental Samples. *J. Food Compos. Anal.* **2024**, *133*, 106426. https://doi.org/10.1016/j.jfca.2024.106426.
63. Ghosh, S.; Mondal, A. Aggregation Chemistry of Green Silver Nanoparticles for Sensing of Hg2+ and Cd2+ Ions. *Colloids Surf. A* **2020**, *605*, 125335. https://doi.org/10.1016/j.colsurfa.2020.125335.

 doi:10.20944/preprints202601.1310.v1

64. Ulloa-Gomez, A. M.; Lucas, A.; Koneru, A.; Barui, A.; Stanciu, L. Simultaneous Colorimetric and Electrochemical Detection of Trace Mercury (Hg2+) Using a Portable and Miniaturized Aptasensor. *Biosens. Bioelectron.* **2023**, *221*, 114419. https://doi.org/10.1016/j.bios.2022.114419.
65. Yang, J.; Feng, L.; Liu, J.; Li, S.; Li, N.; Zhang, X. DNA-Mediated Charge Neutralization of AuNPs for Colorimetric Sensing of Hg2+ in Environmental Waters and Cosmetics. *Sens. Actuators B Chem.* **2024**, *398*, 134697. https://doi.org/10.1016/j.snb.2023.134697.
66. Liu, L.; Ling, Y.; Han, J.; Hao, T.; Li, X. Rapid and Highly Selective Colorimetric Detection of Mercury(Ii) Ions in Water Sources Based on a Ribavirin Functionalized AuNP Sensor. *Anal. Methods* **2022**, *14*, 4669–4679. https://doi.org/10.1039/D2AY01437H.
67. Do Dat, T.; Cong, C. Q.; Le Hoai Nhi, T.; Khang, P. T.; Nam, N. T. H.; Thi Tinh, N.; Hue, D. T.; Hieu, N. H. Green Synthesis of Gold Nanoparticles Using Andrographis Paniculata Leave Extract for Lead Ion Detection, Degradation of Dyes, and Bioactivities. *Biochem. Eng. J.* **2023**, *200*, 109103. https://doi.org/10.1016/j.bej.2023.109103.
68. Zannotti, M.; Piras, S.; Remia, L.; Appignanesi, D.; Giovannetti, R. Selective Colorimetric Detection of Pb(II) Ions by Using Green Synthesized Gold Nanoparticles with Orange Peel Extract. *Chemosensors* **2024**, *12*, 33. https://doi.org/10.3390/chemosensors12030033.
69. Zannotti, M.; Piras, S.; Magnaghi, L. R.; Biesuz, R.; Giovannetti, R. Silver Nanoparticles from Orange Peel Extract: Colorimetric Detection of Pb2+ and Cd2+ Ions with a Chemometric Approach. *Spectroc. Acta Pt. A-Molec. Biomolec. Spectr.* **2024**, *323*, 124881. https://doi.org/10.1016/j.saa.2024.124881.
70. Hladun, C.; Beyer, M.; Paliakkara, J.; Othman, A.; Bou-Abdallah, F. A Simple and Highly Sensitive Colorimetric Assay for the Visual Detection of Lead and Chromium Using Ascorbic Acid Capped Gold Nanoparticles. *Anal. Methods* **2025**, *17*, 15–25. https://doi.org/10.1039/D4AY01924E.
71. Yan, W.; Qin, X.; Sang, X.; Zhou, X.; Zheng, Y.; Yuan, Y.; Zhang, Y. DNAzyme Amplified Dispersion State Change of Gold Nanoparticles and Its Dual Optical Channels for Ultrasensitive and Facile Detection of Lead Ion in Preserved Eggs. *Food Chem.* **2024**, *435*, 137538. https://doi.org/10.1016/j.foodchem.2023.137538.
72. Liu, J.; Yang, H.; Li, H.; Wang, J.; Zhou, X. A Colorimetric Nanobiosensor with Enhanced Sensitivity for Detection of Lead (II) in Real-Water Samples via an Adenine-Cytosine Mismatched DNAzyme. *Front. Environ. Sci. Eng.* **2024**, *18*, 156. https://doi.org/10.1007/s11783-024-1916-0.
73. Kubheka, N. P.; Shange, S. F.; Onwubu, S. C.; Deenadayalu, N.; Mdluli, P. S.; Mokhothu, T. H. ImageJ Analysis for Quantifying Lead Ion in Environmental Water Using Gold Nanoparticles as a Colorimetric Probe. *J. Mol. Liq.* **2025**, *420*, 126804. https://doi.org/10.1016/j.molliq.2024.126804.
74. He, J.; Li, X.; Wang, Y.; Wu, P. SYBR Green I and DNA-Modulated Charge Neutralization Assembly of Naked AuNPs for Fast Colorimetric Sensing of Cd2+ in Cosmetics. *Microchem. J.* **2024**, *200*, 110468. https://doi.org/10.1016/j.microc.2024.110468.
75. Arain, M.; Nafady, A.; Haq, M. A. U.; Asif, H. M.; Ahmad, H. B.; Soomro, R. A.; Shah, M. R. Secnidazole Functionalized Silver Nanoparticles as Trace Level Colorimetric Sensor for the Detection of Cadmium Ions. *Optik* **2024**, *299*, 171620. https://doi.org/10.1016/j.ijleo.2024.171620.
76. Dayanidhi, K.; Sheik Eusuff, N. Distinctive Detection of Fe2+ and Fe3+ by Biosurfactant Capped Silver Nanoparticles via Naked Eye Colorimetric Sensing. *New J. Chem.* **2021**, *45*, 9936–9943. https://doi.org/10.1039/D1NJ01342D.
77. Andreani, A. S.; Nurkhaliza, F.; Ridwan, M.; Daniarti, S. F.; Rosmaniar, L.; Kumalasari, M. R. Unveiling the Role of α- and β-CDs in Gold Nanoparticle Gel-Based Sensors for Fe3+ Colorimetric Detection. *Talanta Open* **2025**, *12*, 100557. https://doi.org/10.1016/j.talo.2025.100557.
78. Patra, S.; Golder, A. K.; Uppaluri, R. V. Monodispersed AuNPs Synthesized in a Bio-Based Route for Ultra Selective Colorimetric Determination of Ni(II) Ions. *Chem. Phys. Impact* **2023**, *7*, 100388. https://doi.org/10.1016/j.chphi.2023.100388.
79. Nubatonis, Y. K.; Roto, R.; Siswanta, D.; Keikimanova, M.; Hosseini-Bandegharaei, A. Smartphone Colorimetry for Rapid Environmental Monitoring: Detecting Ni2+ Using EDTA and Mercapto Succinic Acid Functionalized Silver Nanoparticles. *J. Mol. Liq.* **2025**, *426*, 127351. https://doi.org/10.1016/j.molliq.2025.127351.

 doi:10.20944/preprints202601.1310.v1

80. Wu, L.; Huang, G.; Xie, T.; Zhang, A.; Fu, Y. Green and Ligand-Free Gold Nanoparticles in Padina Australis Extract for Colorimetric Detection of Cu2+ in Water. *Colloids Surf. A* **2023**, *658*, 130773. https://doi.org/10.1016/j.colsurfa.2022.130773.
81. Aqillah, F.; Diki Permana, M.; Eddy, D. R.; Firdaus, M. L.; Takei, T.; Rahayu, I. Detection and Quantification of Cu2+ Ion Using Gold Nanoparticles via Smartphone-Based Digital Imaging Colorimetry Technique. *Results Chem.* **2024**, *7*, 101418. https://doi.org/10.1016/j.rechem.2024.101418.
82. Nguyen, M.-K.; Nguyen, C.-N.-T.; Vo, K.-B. Functionalized Hydrogel-Based Colorimetric Sensor for Cu2+ Detection. *Mater. Res. Express* **2025**, *12*, 075506. https://doi.org/10.1088/2053-1591/adee83.
83. Colford, S.; Dhirani, A.-A. Detection of Cu2+ Ion with 100-Fold Improvement Using Mercaptobenzoic Acid-Capped Au Nanoparticles Purified by pH Selective Precipitation. *Colloids Surf. A* **2025**, *723*, 137416. https://doi.org/10.1016/j.colsurfa.2025.137416.
84. Joshi, P.; Painuli, R.; Kumar, D. Label-Free Colorimetric Nanosensor for the Selective On-Site Detection of Aqueous Al3+. *ACS Sustain. Chem. Eng.* **2017**, *5*, 4552–4562. https://doi.org/10.1021/acssuschemeng.6b02861.
85. Rastogi, L.; Dash, K.; Ballal, A. Selective Colorimetric/Visual Detection of Al3+ in Ground Water Using Ascorbic Acid Capped Gold Nanoparticles. *Sens. Actuators B Chem.* **2017**, *248*, 124–132. https://doi.org/10.1016/j.snb.2017.03.138.
86. Ghodake, G.; Shinde, S.; Kadam, A.; Saratale, R. G.; Saratale, G. D.; Syed, A.; Shair, O.; Alsaedi, M.; Kim, D.-Y. Gallic Acid-Functionalized Silver Nanoparticles as Colorimetric and Spectrophotometric Probe for Detection of Al3+ in Aqueous Medium. *J. Ind. Eng. Chem.* **2020**, *82*, 243–253. https://doi.org/10.1016/j.jiec.2019.10.019.
87. Bezuneh, T. T.; Ofgea, N. M.; Tessema, S. S.; Bushira, F. A. Tannic Acid-Functionalized Silver Nanoparticles as Colorimetric Probe for the Simultaneous and Sensitive Detection of Aluminum(III) and Fluoride Ions. *ACS Omega* **2023**, *8*, 37293–37301. https://doi.org/10.1021/acsomega.3c05092.
88. Montenegro, M. F.; Morales, J. M. N.; Morán Vieyra, F. E.; Borsarelli, C. D. Eco-Friendly Synthesis of a Silver Nanohybrid with Carbon Dots Derived from Quebracho Colorado Leaves and Its Application in the Colorimetric Detection of Al3+. *Spectroc. Acta Pt. A-Molec. Biomolec. Spectr.* **2025**, *343*, 126628. https://doi.org/10.1016/j.saa.2025.126628.
89. Taheri, H.; Khayatian, G. Smartphone-Based Microfluidic Chip Modified Using Pyrrolidine-1-Dithiocarboxylic Acid for Simultaneous Colorimetric Determination of Cr3+ and Al3+ Ions. *Spectroc. Acta Pt. A-Molec. Biomolec. Spectr.* **2022**, *272*, 121000. https://doi.org/10.1016/j.saa.2022.121000.
90. Kim, D.-Y.; Yang, T.; Srivastava, P.; Nile, S. H.; Seth, C. S.; Jadhav, U.; Syed, A.; Bahkali, A. H.; Ghodake, G. S. Alginic Acid-Functionalized Silver Nanoparticles: A Rapid Monitoring Tool for Detecting the Technology-Critical Element Tellurium. *J. Hazard. Mater.* **2024**, *465*, 133161. https://doi.org/10.1016/j.jhazmat.2023.133161.
91. Hussain, K.; Umar, A. R.; Rasheed, S.; Hassan, M.; Laiche, M. H.; Muhammad, H.; Hanif, M.; Aslam, Z.; Shah, M. R. Smartphone-Integrated Resorcinarene Macrocycle Capped Silver Nanoparticles (RMF-AgNPs) Probe for Enhanced La(III) Detection in Diverse Environments. *J. Ind. Eng. Chem.* **2024**, *138*, 256–269. https://doi.org/10.1016/j.jiec.2024.04.001.
92. Hsiao, M.; Chen, S.-H.; Li, J.-Y.; Hsiao, P.-H.; Chen, C.-Y. Unveiling the Detection Kinetics and Quantitative Analysis of Colorimetric Sensing for Sodium Salts Using Surface-Modified Au-Nanoparticle Probes. *Nanoscale Adv.* **2022**, *4*, 3172–3181. https://doi.org/10.1039/D2NA00211F.
93. Berasarte, I.; Bordagaray, A.; Garcia-Arrona, R.; Ostra, M.; Vidal, M. Silver Nanoparticles for the Colorimetric Determination of Electrolytes by UV–Vis Spectrophotometry and Digital Image Analysis. *Sens. Bio-Sens. Res.* **2025**, *49*, 100831. https://doi.org/10.1016/j.sbsr.2025.100831.
94. Patel, M. R.; Upadhyay, M. D.; Ghosh, S.; Basu, H.; Singhal, R. K.; Park, T. J.; Kailasa, S. K. Synthesis of Multicolor Silver Nanostructures for Colorimetric Sensing of Metal Ions (Cr3+, Hg2+ and K+) in Industrial Water and Urine Samples with Different Spectral Characteristics. *Environ. Res.* **2023**, *232*, 116318. https://doi.org/10.1016/j.envres.2023.116318.
95. Frost, M. S.; Dempsey, Michael. J.; Whitehead, D. E. Highly Sensitive SERS Detection of Pb2+ Ions in Aqueous Media Using Citrate Functionalised Gold Nanoparticles. *Sens. Actuators B Chem.* **2015**, *221*, 1003–1008. https://doi.org/10.1016/j.snb.2015.07.001.

 doi:10.20944/preprints202601.1310.v1

96. Xu, Z.; Zhang, L.; Mei, B.; Tu, J.; Wang, R.; Chen, M.; Cheng, Y. A Rapid Surface-Enhanced Raman Scattering (SERS) Method for Pb2+ Detection Using L-Cysteine-Modified Ag-Coated Au Nanoparticles with Core–Shell Nanostructure. *Coatings* **2018**, *8*, 394. https://doi.org/10.3390/coatings8110394.
97. Liu, M.; Zareef, M.; Zhu, A.; Wei, W.; Li, H.; Chen, Q. SERS-Based Au@Ag Core-Shell Nanoprobe Aggregates for Rapid and Facile Detection of Lead Ions. *Food Control* **2024**, *155*, 110078. https://doi.org/10.1016/j.foodcont.2023.110078.
98. Liu, Q.; Wei, Y.; Luo, Y.; Liang, A.; Jiang, Z. Quantitative Analysis of Trace Pb(II) by a DNAzyme Cracking-Rhodamine 6G SERRS Probe on AucoreAgshell Nanosol Substrate. *Spectroc. Acta Pt. A-Molec. Biomolec. Spectr.* **2014**, *128*, 806–811. https://doi.org/10.1016/j.saa.2014.03.008.
99. Chadha, R.; Das, A.; Debnath, A. K.; Kapoor, S.; Maiti, N. 2-Thiazoline-2-Thiol Functionalized Gold Nanoparticles for Detection of Heavy Metals, Hg(II) and Pb(II) and Probing Their Competitive Surface Reactivity: A Colorimetric, Surface Enhanced Raman Scattering (SERS) and x-Ray Photoelectron Spectroscopic (XPS) Study. *Colloids Surf. A* **2021**, *615*, 126279. https://doi.org/10.1016/j.colsurfa.2021.126279.
100. Wang, G. Q.; Chen, L. X. Aptameric SERS Sensor for Hg2+ Analysis Using Silver Nanoparticles. *Chin. Chem. Lett.* **2009**, *20*, 1475–1477. https://doi.org/10.1016/j.cclet.2009.06.029.
101. Hassan, M. M.; Ahmad, W.; Zareef, M.; Rong, Y.; Xu, Y.; Jiao, T.; He, P.; Li, H.; Chen, Q. Rapid Detection of Mercury in Food via Rhodamine 6G Signal Using Surface-Enhanced Raman Scattering Coupled Multivariate Calibration. *Food Chem.* **2021**, *358*, 129844. https://doi.org/10.1016/j.foodchem.2021.129844.
102. Dasary, S. S. R.; Jones, Y. K.; Barnes, S. L.; Ray, P. C.; Singh, A. K. Alizarin Dye Based Ultrasensitive Plasmonic SERS Probe for Trace Level Cadmium Detection in Drinking Water. *Sens. Actuators B Chem.* **2016**, *224*, 65–72. https://doi.org/10.1016/j.snb.2015.10.003.
103. Du, J.; Jing, C. One-Step Fabrication of Dopamine-Inspired Au for SERS Sensing of Cd2+ and Polycyclic Aromatic Hydrocarbons. *Anal. Chim. Acta* **2019**, *1062*, 131–139. https://doi.org/10.1016/j.aca.2019.02.033.
104. Guo, X.; Xiao, D.; Ma, Z.; Zheng, Q.; Wang, D.; Wu, Y.; Ying, Y.; Wen, Y.; Wang, F.; Yang, H. Surface Reaction Strategy for Raman Probing Trace Cadmium Ion. *Arab. J. Chem.* **2020**, *13*, 6544–6551. https://doi.org/10.1016/j.arabjc.2020.06.010.
105. Ye, Y.; Liu, H.; Yang, L.; Liu, J. Sensitive and Selective SERS Probe for Trivalent Chromium Detection Using Citrate Attached Gold Nanoparticles. *Nanoscale* **2012**, *4*, 6442. https://doi.org/10.1039/c2nr31985c.
106. Ly, N.; Joo, S.-W. Silver Nanoparticle-Enhanced Resonance Raman Sensor of Chromium(III) in Seawater Samples. *Sensors* **2015**, *15*, 10088–10099. https://doi.org/10.3390/s150510088.
107. Cheng, W.; Tang, P.; He, X.; Xing, X.; Liu, S.; Zhang, F.; Lu, X.; Zhong, L. Au/Ag Composite-Based SERS Nanoprobe of Cr3+. *Anal. Bioanal. Chem.* **2021**, *413*, 2951–2960. https://doi.org/10.1007/s00216-021-03228-4.
108. Li, F.; Wang, J.; Lai, Y.; Wu, C.; Sun, S.; He, Y.; Ma, H. Ultrasensitive and Selective Detection of Copper (II) and Mercury (II) Ions by Dye-Coded Silver Nanoparticle-Based SERS Probes. *Biosens. Bioelectron.* **2013**, *39*, 82–87. https://doi.org/10.1016/j.bios.2012.06.050.
109. Ly, N.; Seo, C.; Joo, S.-W. Detection of Copper(II) Ions Using Glycine on Hydrazine-Adsorbed Gold Nanoparticles via Raman Spectroscopy. *Sensors* **2016**, *16*, 1785. https://doi.org/10.3390/s16111785.
110. Xu, S.; Cao, X.; Zhou, Y. Polyvinylpyrrolidine-Functionalized Silver Nanoparticles for SERS Based Determination of Copper(II). *Microchim. Acta* **2019**, *186*, 562. https://doi.org/10.1007/s00604-019-3664-6.
111. Wang, C.; Fu, Y.; Li, Y.; Liu, Y.; Wan, R.; Shen, Y. Interference-Free SERS Tags for Copper Ion Sensing upon Hypoxia by in Situ Hot-Spot Generation. *Talanta* **2026**, *297*, 128767. https://doi.org/10.1016/j.talanta.2025.128767.
112. Feng, H.; Fu, Q.; Du, W.; Zhu, R.; Ge, X.; Wang, C.; Li, Q.; Su, L.; Yang, H.; Song, J. Quantitative Assessment of Copper(II) in Wilson's Disease Based on Photoacoustic Imaging and Ratiometric Surface-Enhanced Raman Scattering. *ACS Nano* **2021**, *15*, 3402–3414. https://doi.org/10.1021/acsnano.0c10407.
113. Hsieh, M.-Y.; Huang, P.-J. Magnetic Nanoprobes for Rapid Detection of Copper Ion in Aqueous Environment by Surface-Enhanced Raman Spectroscopy. *RSC Adv.* **2022**, *12*, 921–928. https://doi.org/10.1039/D1RA07482B.
114. Guo, Y.; Li, D.; Zheng, S.; Xu, N.; Deng, W. Utilizing Ag–Au Core-Satellite Structures for Colorimetric and Surface-Enhanced Raman Scattering Dual-Sensing of Cu (II). *Biosens. Bioelectron.* **2020**, *159*, 112192. https://doi.org/10.1016/j.bios.2020.112192.

 doi:10.20944/preprints202601.1310.v1

115. Kumar, P. P. P. Colorimetric and SERS-Based Multimode Detection Platform for Cu(II) Ions Using Peptide–Gold Nanoparticles. *Colorants* **2025**, *4*, 29. https://doi.org/10.3390/colorants4040029.
116. Zheng, S.; Li, D.; Fodjo, E. K.; Deng, W. Colorimetric/Fluorescent/SERS Triple-Channel Sensing of Cu2+ in Real Systems Based on Chelation-Triggered Self-Aggregation. *Chem. Eng. J.* **2020**, *399*, 125840. https://doi.org/10.1016/j.cej.2020.125840.
117. Li, C.; Ouyang, H.; Tang, X.; Wen, G.; Liang, A.; Jiang, Z. A Surface Enhanced Raman Scattering Quantitative Analytical Platform for Detection of Trace Cu Coupled the Catalytic Reaction and Gold Nanoparticle Aggregation with Label-Free Victoria Blue B Molecular Probe. *Biosens. Bioelectron.* **2017**, *87*, 888–893. https://doi.org/10.1016/j.bios.2016.09.053.
118. Guo, X.; Li, M.; Hou, T.; Wu, H.; Wen, Y.; Yang, H. A Novel and Stable Raman Probe for Sensing Fe (III). *Sens. Actuators B Chem.* **2016**, *224*, 16–21. https://doi.org/10.1016/j.snb.2015.10.034.
119. Xu, G.; Li, N.; Sun, Y.; Gao, C.; Ma, L.; Song, P.; Xia, L. A Label-Free, Rapid, Sensitive and Selective Technique for Detection of Fe2+ Using SERRS with 2,2′-Bipyridine as a Probe. *Chem. Eng. J.* **2021**, *414*, 128741. https://doi.org/10.1016/j.cej.2021.128741.
120. Li, J.; Chen, L.; Lou, T.; Wang, Y. Highly Sensitive SERS Detection of As3+ Ions in Aqueous Media Using Glutathione Functionalized Silver Nanoparticles. *ACS Appl. Mater. Interfaces* **2011**, *3*, 3936–3941. https://doi.org/10.1021/am200810x.
121. Charkova, T. Determination of Barium Ions by SERS Using Silver Nanoparticles. *Nano-Struct. Nano-Objects* **2025**, *43*, 101511. https://doi.org/10.1016/j.nanoso.2025.101511.
122. Jin, H.; Itoh, T.; Yamamoto, Y. S. Classification of La3+ and Gd3+ Rare-Earth Ions Using Surface-Enhanced Raman Scattering. *J. Phys. Chem. C* **2024**, *128*, 5611–5620. https://doi.org/10.1021/acs.jpcc.3c05225.
123. Sharma, S.; Jaiswal, A.; Uttam, K. N. Colorimetric and Surface Enhanced Raman Scattering (SERS) Detection of Metal Ions in Aqueous Medium Using Sensitive, Robust and Novel Pectin Functionalized Silver Nanoparticles. *Anal. Lett.* **2020**, *53*, 2355–2378. https://doi.org/10.1080/00032719.2020.1743715.
124. Sharma, S.; Jaiswal, A.; Uttam, K. N. Synthesis of Sensitive and Robust Lignin Capped Silver Nanoparticles for the Determination of Cobalt(II), Chromium(III), and Manganese(II) Ions by Colorimetry and Manganese(II) Ions by Surface-Enhanced Raman Scattering (SERS) in Aqueous Media. *Anal. Lett.* **2020**, *54*, 2051–2069. https://doi.org/10.1080/00032719.2020.1837855.
125. Sharma, S.; Jaiswal, A.; Uttam, K. N. Determination of Chromium(VI), Chromium(III), Arsenic(V), Aluminum(III), Iron(II), and Manganese(II) by Colorimetry and Surface-Enhanced Raman Scattering (SERS) Using Ferulic Acid Functionalized Silver Nanoparticles. *Anal. Lett.* **2021**, *55*, 715–727. https://doi.org/10.1080/00032719.2021.1963269.
126. Daublytė, E.; Zdaniauskienė, A.; Talaikis, M.; Charkova, T. Synthesis and Functionalization of Silver Nanoparticles for Divalent Metal Ion Detection Using Surface-Enhanced Raman Spectroscopy. *J. Nanopart. Res.* **2023**, *26*, 6. https://doi.org/10.1007/s11051-023-05917-w.
127. Kappen, J.; Bharathi, S.; John, S. A. Probing the Interaction of Heavy and Transition Metal Ions with Silver Nanoparticles Decorated on Graphene Quantum Dots by Spectroscopic and Microscopic Methods. *Langmuir* **2022**, *38*, 4442–4451. https://doi.org/10.1021/acs.langmuir.2c00273.